Leptin Antagonism Inhibits Prostate Cancer Xenograft Growth and Progression.

Lisa K Philp[1], Anja Rockstroh[1], Martin C Sadowski[1], Atefeh Taherian Fard[1], Melanie Lehman[1], Gregor Tevz[1], Michelle S Libério[1], Charles L Bidgood[1], Jennifer H Gunter[1], Stephen McPherson[1], Nenad Bartonicek[2], John D Wade[3,4], Laszlo Otvos Jr[5,6], Colleen C Nelson[1].

[1]Australian Prostate Cancer Research Centre - Queensland, Institute of Health and Biomedical Innovation, School of Biomedical Sciences, Queensland University of Technology, Princess Alexandra Hospital, Translational Research Institute, Brisbane, QLD, Australia; [2]Garvan Institute of Medical Research, Sydney, NSW, Australia; [3]Florey Institute of Neuroscience and Mental Health, University of Melbourne, Melbourne, VIC, Australia; [4]School of Chemistry, University of Melbourne, Melbourne, VIC; [5]OLPE, LLC, Audubon, PA, United States; [6]Institute of Medical Microbiology, Semmelweis University, Budapest, Hungary.

Corresponding author:

Dr Lisa K Philp, Australian Prostate Cancer Research Centre - Queensland, Level 1, Building 33, Princess Alexandra Hospital, 199 Ipswich Rd, Brisbane, 4102, Australia.

Email: lisa.philp@qut.edu.au.

Running title: Effective new antitumor therapy targeting LEPR

Keywords: Leptin receptor antagonist, Allo-aca, prostate cancer, leptin, peptide drug

Word count: 5398

Abstract:

Hyperleptinemia is a well-established therapeutic side-effect of drugs inhibiting the androgen axis in prostate cancer (PCa), including main stay androgen deprivation therapy (ADT) and androgen targeted therapies (ATT). Given significant crossover between the adipokine hormone signalling of leptin and multiple cancer-promoting hallmark pathways, including growth, proliferation, migration, angiogenesis, metabolism and inflammation, targeting the leptin axis is therapeutically appealing, especially in advanced PCa where current therapies fail to be curative. In this study we uncover leptin as a novel universal target in PCa, and are the first to highlight increased intratumoural leptin and leptin receptor (LEPR) expression in PCa cells and patient tumours exposed to androgen deprivation, as is observed in patient tumours of metastatic and castrate resistant (CRPC) PCa. We also reveal world-first preclinical evidence that demonstrates marked efficacy of targeted leptin signalling blockade, using Allo-aca, a potent, specific, and safe LEPR peptide antagonist. Allo-aca suppressed tumour growth and delayed progression to CRPC in mice bearing LNCaP xenografts, with reduced tumour vascularity and altered pathways of apoptosis, transcription/translation, and energetics in tumours determined as potential mechanisms underpinning anti-tumour efficacy. We highlight LEPR blockade in combination with androgen axis inhibition represents a promising new therapeutic strategy vital in advanced PCa treatment.

Introduction:

Prostate cancer (PCa) is androgen-dependent and consequently drugs inhibiting multiple facets of the androgen axis are used as therapeutics (Harris et al., 2009). However, in advanced PCa, tumours develop mechanisms to escape the pressure of androgen receptor (AR) targeting (Tilki et al., 2016, Sharifi, 2013). Treatment failure through reactivation of AR is one of the greatest challenges faced in treating advanced PCa, ultimately contributing to the development of castration resistant PCa (CRPC). Additionally, androgen deprivation/targeted therapies (ADT/ATT) lead to patient development of Metabolic Syndrome-like symptoms, including sarcopenic adiposity and raised circulating lipids and metabolic hormones, insulin and leptin (Basaria et al., 2006, Faris and Smith, 2010). Adipokine leptin,

primarily secreted from adipose tissue, is best known for its role in obesity, satiety and in regulating energy homeostasis; however evidence suggests a critical adverse role in cancer (Otvos et al., 2011, Vansaun, 2013). Circulating leptin is increased 2-fold in PCa patients compared to healthy individuals, and elevated a further 2-fold in those patients undergoing ADT (Basaria et al., 2006). Hyperleptinemia in PCa is of concern as leptin exposure has been linked to increased proliferation of androgen-dependent and -independent PCa *in vitro* (Habib et al., 2015, Noda et al., 2015, Sarmento-Cabral et al., 2017, Somasundar et al., 2003, Xu et al., 2020, Gorrab et al., 2020). Conversely, suppression of leptin signalling by leptin receptor (LEPR, OBR) knockdown elicited anti-proliferative effects *in vitro* (Noda et al., 2015). In addition to promoting cell growth, leptin has been demonstrated to suppress apoptosis, promote migration, and increase cellular angiogenic and invasive factors in PCa cell lines (Sarmento-Cabral et al., 2017, Frankenberry et al., 2004, Gorrab et al., 2020, Somasundar et al., 2004, Xu et al., 2020); all of which are factors that contribute to the cellular survival, tumour burden and more rapid progression of PCa. To date all studies have assessed the impact of leptin in a purely androgen-rich *in vitro* environment. However, given circulating leptin is highest in PCa following anti-androgens (Basaria et al., 2006), and leptin alone can raise PSA secretion in androgen-sensitive PCa cells (Sarmento-Cabral et al., 2017), understanding the role of leptin in PCa progression following anti-androgen treatment, and in regards to therapy resistance, is of critical importance. As is studying leptin and androgen axis *in vivo*, due to the complexities inherent to these two endocrine signalling axes and their potential for both systemic and intratumoural impacts.

Our study is the first to assess the impact of leptin in PCa under androgen-deprived conditions and the consequences of LEPR signalling blockade using a selective and potent LEPR antagonist Allo-aca (Otvos et al., 2014, Otvos et al., 2011) in preventing hallmarks of PCa progression *in vivo*. In this study we demonstrated, in addition to hyperleptinemia (Basaria et al., 2006), intratumoural leptin and its receptor are increased following androgen deprivation. We report pharmacological blockade of leptin signalling was efficacious in significantly reducing tumour burden and delaying progression to CRPC *in vivo*. Strong anti-tumour efficacy in mice provides rationale for further investigation and development of Allo-aca as a potential ADT/ATT co-therapeutic with real translational potential.

Methodology:

Ethics statement

The use of animals was approved by the University of Queensland and Queensland University of Technology (QUT) Animal Ethics Committees (QUT/TRI-353-17). Animal studies were conducted in accordance with the Australian Code of Practice for the Care and Use of Animals for Scientific Purposes, institutional and ARRIVE guidelines. Cell line use was approved by QUT Human Research Ethics Committee.

LEP and LEPR expression in public patient datasets

Expression (log2 median-centred intensity; log2 copy number units) were assessed using Oncomine (ThermoFisher Scientific, Seventeen Mile Rocks, AUS), or cBioPortal (https://www.cbioportal.org/).

AR ChIPseq peak analysis

Analysis of ChIPseq data, accessed via Cistrome, identified AR ChIPseq peaks enriched in regions 5KB upstream and also in a 25KB window around Genecode transcripts, undertakenas described in (Tousignant et al., 2019).

In vitro cell culture and treatments

LNCaP (CVCL_0395), VCaP (CVCL_2235), LAPC4 (CVCL_4744) and C4-2B (CVCL_4784) cells were sourced from American Type Culture Collection (Manassas, USA); DuCaP cells were generously donated by Dr Matthias Nees (Turku University, Finland). Cell lines were regularly mycoplasma tested and authenticated by short tandem repeat DNA profiling (Dec-2017, Mar-2018, Dec-2020; Genomics Research Centre (Brisbane, AUS)). Growth media (phenol-red free) was RPMI supplemented with fetal bovine serum (FBS) (5%FBS: LNCaP, C4-2B; 10%FBS VCaP, DuCaP) or Iscove's Modified Dulbecco's Medium + 5%FBS + dihydrotestosterone (DHT; 10nM) (LAPC4) (Life Technologies, Mulgrave, AUS)).

To model acute androgen deprivation (ADT) cells were seeded in growth media (72hr) before switching to media containing charcoal-stripped serum (CSS) or serum-free media (SFM) plus 0.2% bovine serum

albumin (BSA) (Sigma-Aldrich, St Louis, USA). ATT enzalutamide (ENZ; 10μM) was provided for 48hr (Selleck Chemicals, Houston, USA). Androgen-replete conditions were achieved by supplementing ADT-media with DHT or R1881 (1nM) for 48hr. Long-term ADT was achieved over 10d with CSS-media (refreshed every second day); from which, media was supplemented daily with DHT or Vehicle (Veh) for 6d.

Induction/repression of leptin signalling was achieved using human recombinant leptin (R&D Systems, Minneapolis, USA) and LEPR antagonist, Allo-aca (generously provided by Profs Laszlo Otvos and John Wade; also known as ARV-1802), respectively (Veh: sterile saline (0.9%)).

In vitro AR knockdown

Doxycycline-inducible AR and control non-targeting (NT) shRNA lentiviral vectors were purchased from Dharmacon Inc (Millennium Science, Musgrave, AUS; shAR-6 [V2THS_149847]). shAR and shNT LNCaP were generated as described (Tevz et al., 2016). shRNA induction was performed using 1μg/mL doxycycline (Dox; Sigma-Aldrich). *LEP* and *LEPR* were assessed by RNAseq. Efficient AR mRNA knockdown (+Dox) is demonstrated in **Fig2**.

Cell growth

Growth was assessed using 2-hourly live imaging (IncuCyte FLR (Essen Bioscience, Ann Arbor, USA) and poly-L-ornithine pre-coated Essen ImageLock plates (Sadowski et al., 2014)). Cells were seeded in ADT-media and after 48hrs treated (leptin ± Allo-aca in ADT-media). Data are represented as confluence relative to pre-treatment. CyQUANT Proliferation Assays (ThermoFisher) determined cellular number post-treatment and were expressed relative to pre-treatment.

Transwell migration

Cells were seeded in growth media (72hr) in T25 flasks, subjected to 48hr CSS-media, then supplemented with leptin ± Allo-aca (24hr). Cells were dissociated, resuspended in SFM ± treatments and 100,000 cells seeded onto a transwell insert (Millipore, Merck, Germany) in a 24-well plate above FBS-chemoattractant. Cells were allowed migration time based on migratory capacity (20hr, C4-2B;

42hr, LNCaP); then fixed, Quickdip stained (ScyTek Laboratories, Logan, USA) and captured by light microscopy (5 fields-of-view) with migrating cells counted.

Alpha screen

Cells were treated as above and subjected to leptin ± Allo-aca, vehicle (DMSO) or ERK inhibition (UO126) control. Lysates were assayed by alpha screen for cellular quantitation of phosphorylation of ERK1/2 as per instructions (PerkinElmer, Waltham, USA).

Measurement of LEPR by Immunofluorescence

In 96-well format (Cellvis optical plate), LNCaP cells pre-subjected to androgen deplete (CSS-media) or enriched (growth media) conditions, were treated with 10nM leptin ± 100nM Allo-aca (30min). Cells were then washed, fixed (10% neutral buffered formalin, 6min) and permeabilised (PBS +0.1% Triton-X-100, 10min). Cells were blocked (30min) in PBS containing 1%BSA, 0.1%Tween-20 and 22mg/mL glycine and subjected to primary antibody (1:200) in blocking buffer (Santa Cruz ObR sc8391; 45min). After washing, cells were incubated with secondary antibody (Alexa-Fluor-488 1:2000) and DNA counterstained using DAPI (ThermoFisher Scientific). Primary antibody omission served as a negative control. >500 cells/well were imaged using confocal InCell 6500HS High Content Analysis system (Cytiva). Quantitative analysis was undertaken using CellProfiler Software (v4.07, Broad Institute; ~1,500 cells/treatment (triplicate wells)).

Prostate Cancer Progression Xenograft Model

6-week-old male BALB/c-Foxn1nu/Arc mice (Animal Resource Centre (Murdoch, AUS)) were group housed and fed standard chow (Specialty Feeds, Glen Forrest, AUS) and water *ad libitum* as described previously (Philp et al., 2020). Anaesthetised (isoflurane) mice were injected subcutaneously (s.c.; right-flank) with $1x10^6$ LNCaP cells (p31(+6)) as described by Philp and colleagues (Philp et al., 2020). Body weight and tumour volume (digital callipers) were monitored thrice weekly and weekly values averaged. Weekly isolated serum (submandibular bleed <0.5% weight) tracked PCa progression biomarker, human prostate specific antigen (PSA), secreted solely by xenografts. At PSA ~30-

50ng/mL, anaesthetised mice were castrated and carprofen analgesic (4µg/g) administered pre- and post-surgery. One-week post-castration, mice were randomised to drug; receiving either 1) 1mg/kg Allo-aca or 2) Veh (saline) s.c. daily. Treatment continued until endpoint, determined by 1) maximum tumour volume 1000 mm^3 or 2) AEC-approved welfare score deeming condition required euthanasia necessary (Maugham et al., 2017), whichever was soonest. Tumour volume and doubling time were calculated as previously described (Philp et al., 2020). At endpoint, anaesthetised mice underwent terminal cardiac bleeds. Xenografts and key organs of toxicopathological and metabolic interest were rapidly dissected and weighed post-mortem. Halved tissues were snap frozen (LN_2; stored at -80°C) or formalin-fixed. Formalin-fixed tissues were processed and embedded in paraffin (FFPE).

Live ultrasound-based tumour imaging.

Anaesthetised mice were secured in a lateral position with the right flank facing upward for perpendicular imaging of the tumour. The entire tumour was imaged (0.197mm step size) in 3D using B-mode ultrahigh-resolution ultrasound (US) with a frequency of 30MHz. Photoacoustic (PA) imaging was also performed using the Vevo2100 High Resolution Imaging System (680-970nm wavelength range), LZ400 probe (30 MHz) and LAZRTight unit (VisualSonics, Toronto, Canada) and Oxy-Hemo mode to assess tumour oxygen saturation (sO2) acquired at wavelength 750 nM (Wang et al., 2020). Contrast-enhanced ultrasound US imaging was performed as described previously (Wang et al., 2020) following intravenous bolus of non-targeted microbubbles (VisualSonics) and destruction replenishment perfusion modelling assessed using VevoCQ tool (VevoLab software). Tumour heat maps represent replenishment according to mean transit time (smTT).

ELISA

Total human PSA (GenWay, San Diego, USA), and endpoint adipokines (mouse Leptin and Adiponectin (Millipore, Vienna, Austria)) were assayed in sera as per instructions.

Immunohistochemistry (IHC)

FFPE sections were haematoxylin and eosin (H&E) stained for morphology. IHC of tumours was performed as described by Philp *et al* (Philp et al., 2016), with variations; blocking using CAS-Block (Invitrogen, Paisley, UK); protein visualization by Dako EnVision+ Dual Link System-HRP and Dako Liquid DAB+. Sections were subjected to 4°C overnight incubation with Ki-67 antibody (1:150 (MIB-1; Agilent, Santa Clara, USA)) or primary antibody omission on a serial section (negative control, Matching -1°). Sections were scanned (40x) by Olympus VS120 Slidescanner Microscope (Shinjuku-ku, Japan).

IHC scoring was performed blinded in 8 random regions of interest (ROI) per tumour. Detection thresholds were programmed in QuPath software (Bankhead et al., 2017) to identify cells by staining intensity, with intense (3+), moderate (2+) and low (1+) staining, as well as cells weak/negative for DAB. Area of ROI covered by each intensity was calculated and represented relative to the total ROI area (RA). IHC score was calculated using: [RA weak/negative] + [2*RA low] + [3*RA moderate] + [4*RA intense] and scores across 8 tumour ROIs averaged.

RNA extraction

~20mg xenograft was homogenized by pre-cooled TissueLyser (Qiagen, Germantown, USA; stainless-steel beads, 2-3min, ~20Hz). Homogenate was centrifuged (1min, 10000rpm, 4°C) and supernatant subjected to total RNA extraction (Total RNA Purification Plus; RNase-Free DNase I Kits (Norgen Biotek, Thorold, Canada)). Eluted RNA quality and quantity was assessed NanoDrop. Cells were similarly extracted minus TissueLyser homogenisation.

mRNA sequencing (RNAseq)

Total RNA was further assessed for quality and quantity by Agilent-2100 Bioanalyzer and Qubit®.2.0 Fluorometer, with quality cut-off at RNA integrity number>8. Kinghorn Centre for Clinical Genomics (KCCG, Darlinghurst, AUS) performed library preparation (1µg RNA; Illumina TruSeq Stranded mRNA kit) and RNAseq using paired-end sequencing on an Illumina HiSeq2500 v4.0, multiplexing 6 samples/lane, yielding ~49M reads/sample. Raw data was processed and analysed for differential expression (DE) between treatments as described (Tousignant et al., 2019, Philp et al., 2020), defined

by an absolute fold change of ≥1.5 and a false-discovery rate (FDR) corrected *P*-value ≤0.05. Suppl Fig1 demonstrates the separation of Allo-aca- and Vehicle-treated human tumour transcripts, clustered by PCA and COA plot. Functional annotation and gene network analysis of DE transcripts was performed using Ingenuity Pathway Analysis (Qiagen) or MetaboAnalyst (www.metaboanalyst.ca). A significance cut-off was used for Z-score>2 and <-2 and –log*P*>1.3. Variation between samples and associations scores between the transcriptome of each treatment was assessed by Partial Least Squares Discriminant Analysis (PLS-DA; mixOmics). Xenograft cell deconvolution was performed using CTen (Shoemaker et al., 2012) and gene set signature scoring (GSVA Rpackage; ssGSEA algorithm) using prostate adenocarcinoma-specific ConsensusTME gene set converted to mouse gene symbols. Heatmaps were created in Morpheus (https://software.broadinstitute.org/morpheus).

Microarray gene expression

RNA from a past mouse xenograft model of LNCaP CRPC progression (Locke et al., 2008) was subjected to microarray profiling using a custom 180K Agilent oligo microarray (VPCv3, ID032034, GEO:GPL16604) (Sieh et al., 2012). DE probes between groups were defined as above.

qRT-PCR

Total RNA (1µg) was subjected to cDNA synthesis (SensiFast kit (Bioline, Eveleigh, AUS). qRT-PCR was performed using Applied Biosystems SYBR-Green Master Mix and ViiA-7 Real-Time PCR system (Foster City, US). Relative mRNA levels were determined by comparative ΔΔCt, where expression was normalized relative to housekeeping gene RPL32 and expressed as fold change relative to control. Experiments validating LEPR expression post-ADT were performed in independent duplicates or triplicates. Primer sequences were: LEPR-FWD "5'-CGTGGCATTATCCTTCAGTGG", LEPR-REV "5'-CCAATGTAACAAAACCACACAGAA"; RPL32-FWD "5'-GCACCAGTCAGACCGATATG"; RPL32-REV "5'-ACTGGGCAGCATGTGCTTTG".

Western blot

Tissue was TissueLyser homogenized and extracted as described (Philp et al., 2016, Philp et al., 2008), but in ice-cold RIPA-buffer with Roche cOmplete Protease Inhibitor and PhosphoSTOP tablets (Sigma-Aldrich). 20-35µg total protein, assessed by Pierce BCA assay, was separated by SDS-PAGE using Bolt 4-12%Bis-Tris Gels (ThermoFisher) as detailed by Philp *et al* ((Philp et al., 2020). Nitrocellulose membrane was utilized for blotting transfer, membranes blocked and then probed overnight (4°C) in primary antibody. Following washing, membranes were then incubated with secondary antibody and fluorescent signal detected by Odyssey imaging following a final washing step. Signal quantification was assessed relative to background using ImageStudio. Loading control Vinculin ((sc73614), Santa Cruz Biotechnology (Dallas, US)) unchanged by treatment, was used to normalise target protein abundance. Antibodies used were purchased from Santa Cruz or Cell Signaling (Danvers, USA) (pERK1/2 sc23759, p44/42-MAPK (ERK1/2) 9120S; LEPR sc8391; cleaved caspase-3 9661S; caspase-3 9662S; SREBP-1 sc366; AMPKα 2793; phospho-AMPKα 2535 and VEGF sc57496).

Statistics

Statistical analyses and graphics were performed using Graphpad Prism (v7.0; San Diego, USA) and/or IBM SPSS (v23; Armonk, USA) and RStudio server (v1.1.456; Boston, USA). Unless stated, cell experiments were the average of triplicate technical replicates performed over three biological repeats. Data was checked for normality (Shapiro-wilk) and homogeneity of variance (Levene's test). Comparison of effects between two groups was determined by two-tailed T-test (± Welch's correction if non-homogenous variance); while effects between >two groups was assessed by One-way ANOVA (Sidak post-hoc). If non-normally distributed, an appropriate non-parametric test was performed (Kruskal-Wallis). Two-way ANOVA, with pairwise comparisons (Sidak/ Dunnett's T3), was used to determine the effect of treatment, time and their interaction in progression data. A Gehan-Breslow-Wilcoxon test was used to assess model progression and survival to ethical endpoint. Data are reported as mean ± SEM, unless specified, and $P \leq 0.05$ considered significant.

Results:

LEP and LEPR expression in PCa: patient samples, androgen axis manipulation in vitro and in vivo

Both leptin (*LEP*) (**Fig1A**) and leptin receptor (*LEPR*) (**Fig1B**) are increased in patient samples of primary PCa compared to non-malignant prostate, and their expression rises with increasing Gleason score. *LEP* and *LEPR* are further increased in metastatic samples (vs localised disease), and in patients experiencing PCa recurrence. Similarly, in locally advanced or metastatic patient tumours, ~22wks ADT increased *LEPR* expression in all tumours sequenced (7/7), compared to pre-ADT levels (**Fig1C**). *LEPR* was greatest in metastases of the bone and liver (**Fig1D**), and tended to be higher in aggressive tumours with increasing NEPC (neuroendocrine PCa) score.

When assessed in multiple AR-positive human PCa cell lines subjected to ADT/ATT, *LEPR* was upregulated through inhibition of the androgen axis (**Fig2**). A dramatic increase in *LEPR* mRNA was observed following androgen depletion by CSS in LNCaP, DuCaP and VCaP cells (P<0.0001; **Fig2A**), by ENZ in LNCaP cells (P<0.0001; **Fig2B**), and by inducible knockdown of the AR (shAR) in LNCaP cells (P<0.05; **Fig2C**). Returning androgen-deprived cells to androgen-replete conditions (R1881 or DHT) caused significant *LEPR* repression (P<0.05; **Fig2A,B**). Similarly, *in vivo*, subjecting LNCaP xenografts to ADT by castration produced a marked increase in tumour *LEPR*, compared to intact mice (**Fig2D**). Raised LEPR levels were highest in tumours corresponding to prostate specific antigen (PSA) nadir (P<0.001; when androgen-regulated PCa biomarker PSA is at its lowest in circulation) but remained significantly elevated into development of CRPC (P<0.05). ADT-induced transcriptomic changes in *LEPR* expression were validated by qRT-PCR in two further LNCaP models (**Fig2E**). Acute ADT increased *LEPR* mRNA 4-fold, compared to androgen-replete conditions; while chronic ADT increased *LEPR* up to 9.2-fold, which was rapidly suppressed to 2.6-fold following reintroduction of androgens. These observations were confirmed at the protein level in LNCaP cells subjected to acute ADT, where LEPR abundance increased ~2-fold with ADT (**Fig2F**). When combined with LEPR agonism (leptin) and/or LEPR antagonism (Allo-aca), LEPR abundance remained unchanged from ADT-alone. This was echoed at the mRNA level, where *LEPR* expression was altered by targeting the AR axis (as observed in **Fig2A-E**), with no statistically significant impact of LEPR agonism or antagonism on *LEPR* in the androgen-deprived setting (**Fig2G**).

While androgen axis manipulation significantly influences LEPR expression in AR-positive PCa cell lines, the field's understanding of AR regulation of the leptin axis is limited in PCa. We therefore undertook comprehensive analysis of AR binding sites within a 25kb window of the gene sequence and a 5kb window upstream of the protein start codon of LEP and LEPR using AR ChIPseq data from LNCaP cells treated with AR antagonist bicalutamide (Ramos-Montoya et al., 2014). As shown in **Fig 3A**, LEPR showed enrichment of AR ChIPseq peaks in the 5kb and 25kb windows, while LEP displayed enrichment in the 25kb window alone, which were each abrogated by the presence of bicalutamide. This is corroborated across multiple datasets assessed in Cistrome where AR displayed marked regulatory potential of LEPR, as a promoter-type transcription factor and enhancer-type transcription factor, through AR ChIPseq peak enrichment within 1kb and 10kb of LEPR transcription start, respectively **(Fig 3B)**. AR regulation of LEPR was further confirmed in the AR-positive androgen-sensitive VCaP cell line, where AR function was blocked using two novel small molecule AR antagonists, compared to androgen (R1881) alone (Zhu et al., 2012). Here, AR antagonism reduced AR ChIPseq peak height by approximately half, compared to androgen (**Fig 3C**). These data support a role for AR in regulating the leptin signalling axis.

Targeting LEPR in PCa: Anti-tumour activity of Allo-aca *in vivo*

Given the rise in *LEPR* and *LEP* expression in tumours following ADT/ATT and with PCa progression; alongside well-established systemic hyperleptinemia (Basaria et al., 2006), we investigated the impact of targeting LEPR with Allo-aca in androgen-sensitive LNCaP xenografts. This model of PCa progression was selected due to a well-defined consistent response to castration where PSA decreases and nadirs a week post-castration, followed by a progressive increase 2-3wks later to castrate-resistance (CRPC) in mice bearing subcutaneous LNCaP xenografts (Ettinger et al., 2004).

Allo-aca significantly slowed LNCaP xenograft growth, observed in a 4-fold increase in tumour doubling time ($P \leq 0.05$; **Fig4A**), and 2-fold decrease in endpoint tumour volume and mass, compared to Vehicle (Veh, $P \leq 0.05$; **Fig4B,C**). Matched time-points at 15wks post-castration, demonstrate a 6-fold difference in tumour volume between Allo-aca and Veh. Concomitant lowering of serum PSA was

also observed with Allo-aca but failed to reach significance at ethical endpoint (P=0.07; **Fig4D**). Time to PSA recurrence also tended to be delayed in Allo-aca-treated animals (vs Veh, P=0.07; **Fig4E**). Allo-aca-treated mice demonstrated delayed tumour progression curves according to tumour volume and serum PSA from castration (**Suppl Fig 2A,B)**. In a subgroup of mice (50%), Allo-aca treatment elicited tumour regression (**Suppl Fig 2C**) an effect not seen in Veh-treated LNCaP xenografts. In the mice with Allo-aca-regressed tumours, serum PSA remained near nadir levels (**Suppl Fig 2D**). Complete regression without recurrence was observed in 2 mice (20% of n=10). In both Veh and Allo-aca-treated mice, as expected, PSA and tumour volume at endpoint was significantly correlated (Veh r^2=0.44, P=0.04; Allo r^2=0.85, P=0.0004; **Suppl Fig 2E**). Allo-aca prolonged time to ethical endpoint, with time on treatment increased (vs Veh, $P \leq 0.05$; **Fig4F**). This was confirmed by survival to ethical endpoint, where Allo-aca-treated mice progressed to endpoint at a ~2-fold slower rate than Veh ($P \leq 0.05$; **Fig4G**). Prior to treatment, groups exhibited matched time to castration (P=0.5; **Fig4H**); therefore, changes in the tumour growth trajectory or prolonged time on treatment do not stem from variations in the model's initiation trajectory.

Allo-aca increased time on treatment without impacting physiology *in vivo*

As leptin inhibition may be predicted to have systemic effects on the physiology and organs, we performed a detailed analysis. Body weight was unaffected by Allo-aca over chronic treatment (no treatment-by-time effect, P=1.0;) and remained unchanged at endpoint (vs Veh, P=0.6; **Fig5A**). Typically, weight peaked prior to castration, and in the weeks post-castration loss of body condition was observed in all animals, eventually leading to ethical endpoint (delayed by Allo-aca, **Fig3)**. Allo-aca has previously been demonstrated to elicit no toxicological impact up to 50 mg/kg (acute bolus (Otvos et al., 2011)). Similarly, chronic daily Allo-aca had no effect on the absolute weights of a panel of major classical toxicological and metabolic organs (**Fig5B)**, nor when expressed relative to body weight (data not shown). H&E-stained tissues demonstrated no abnormal pathology with Allo-aca (**Fig5J**). Endpoint serum leptin trended higher in Allo-aca compared to Veh (P=0.07; **Fig5C**), however this may be consequential of the sex hormone-dependent nature of leptin (Jenks et al., 2017) or a positive feedback loop in response to LEPR antagonism. In line with this, we found that endpoint leptin

correlated with time on treatment (R^2=0.47, P≤0.001; **Fig5D**) and serum PSA at endpoint (R^2=0.31, P≤0.01; **Fig5E**). When corrected for time on treatment, serum leptin was unchanged from Veh (P=0.9; **Fig5F**). However, based on linear regression analyses other factors are likely contributing to the increased leptin levels observed and this warrants future investigation. Another adipokine, adiponectin, which plays a major role in metabolism and maintaining insulin sensitivity was unaltered in serum following Allo-aca (vs Veh, P=0.2; **Fig5G**) and was not correlated to time on treatment (R^2=0.02, P=0.5; **Fig5H**), nor serum PSA (R^2=0.04, P=0.4; **Fig5I**).

Allo-aca treatment inhibits LNCaP xenograft growth: impacts cell survival and death

Given the tumour growth inhibition observed with Allo-aca, changes in cell cycle, survival or apoptotic markers were investigated. RNAseq was used to assess Allo-aca impact on the tumour transcriptome to identify deregulated molecular pathways that underpin phenotypic changes observed. 1448 human transcripts were DE (521-downregulated, 927-upregulated) with Allo-aca . Apoptosis was a key pathway identified by pathway analysis of Allo-aca DE transcripts (-log$P$=3.31, z=+1.94, **Fig6A**). A generalized induction of pro- and suppression of anti-apoptotic genes with Allo-aca treatment was observed; while hierarchical clustering of apoptotic genes effectively separated Allo-aca from Veh (**Fig6B)**. In keeping with increased apoptosis with Allo-aca treatment, gene set signatures associated with apoptosis, and even cellular senescence, were positively enriched in the Allo-aca-treated tumour transcriptome, compared to Veh **(Fig6C)**. This too is supported by significant top IPA toxicological pathways in Allo-aca-treated tumours featuring Necrosis and Cell Death (renal (P<0.00007, 51/550 molecule overlap); cardiac (P<0.0009, 29/294 overlap); data not shown). Pro-apoptotic induction was validated at the protein level by assessing cleavage (activation) of apoptotic marker, Caspase-3. Increased cleaved Caspase-3 was observed in Allo-aca-treated tumours, (vs Veh; P=0.009, **Fig6D**), while Pro-Caspase-3 was unaffected (P=0.99). The ratio of activated cleaved to pro-form Caspase-3 was also greater with Allo-aca (P=0.018, **Fig6D**). Several other pathways impacting cell viability were identified as significantly impacted by Allo-aca (**Fig6E**), including "Role of CHK proteins in Cell Cycle Checkpoint Control" (-log$P$=2.56, z=+2.12) and "Cyclins and Cell Cycle Regulation" (-log$P$=2.98, z=-1.00). Despite this, marker of cellular proliferation, Ki-67, was unchanged at the protein and RNA level

(*P*=0.6; **Fig6F**). However, this was assessed only using sizable tumours with adequate material for FFPE and RNA extraction; failing to incorporate many of tumours demonstrating regression.

To further explore the impact of Allo-aca on PCa growth, we investigated impacts of leptin and Allo-aca on growth using a panel of cell lines grown in ADT media in 2D-monoculture. Under two androgen-deprived conditions, a dose escalation of 0.5-50nM leptin over 72h failed to alter the growth of AR-positive PCa cell lines with varying levels of androgen-sensitivity (LNCaP, DuCaP, LAPC4 and C4-2B; *P*=0.12-1.0; **Fig7A**). Likewise, antagonism with Allo-aca, alone or in combination with leptin, had no effect on confluence in the escalating doses tested (*P*=0.35-1.0; Allo-aca 0.1-1000nM). Similarly, cells subjected to Enzalutamide failed to demonstrate leptin- or Allo-aca-induced growth effects (**Fig7B**). Cell number was also relatively unaffected by leptin and Allo-aca, however in some cases leptin, but not Allo-aca, tended to increase relative cell number (**Fig7C**). While Allo-aca significantly impacted tumour growth *in vivo,* little impact was observed on cell viability *in vitro.* Targeted LEPR inhibition by Allo-aca, as described previously, was confirmed by measuring the impact of acute Allo-aca exposure in the presence of leptin, compared to leptin alone, on cellular LEPR protein **(Suppl Fig3)** and downstream leptin signalling (**Fig7F)** in LNCaP cells. Here, Allo-aca significantly lowered LEPR cellular integrated intensity by immunofluorescence, compared to the increased LEPR intensity observed with leptin treatment alone (Suppl Fig3). The Raf/MEK/ERK pathway is well-established as critical in cell cycle progression and regulation of apoptosis (De Marinis et al., 2004). As ERK1/2 signalling is downstream of LEPR activation, we assessed ERK1/2 post-Allo-aca treatment. In Allo-aca-treated tumours, "ERK/MAPK Signalling" was one of the top dysregulated pathways identified (-log*P*=4.57, z=1.61; **Fig7D**). Western blot of ERK1/2 in endpoint tumours demonstrated a slighttrend to decreased phospho-ERK1/2 (*P*=0.10) and reduced ratio of phospho:total ERK1/2 (*P*=0.12) with Allo-aca, but failed to reach statistical significance, whilst total ERK1/2 was unchanged (*P*=0.76; **Fig7E**). *In vitro* LNCaP cells exposed to Allo-aca, in the presence of leptin, demonstrated decreased phospho-ERK by alpha screen in comparison to leptin alone, which conversely increased ERK phosphorylation (*P*<0.01; **Fig7F**). The relatively weak response in ERK protein phosphorylation *in vivo*, as compared to acute Allo-aca treatment *in vitro,* could be influenced by chronic responsiveness to Allo-aca with extended treatment which ranged anywhere from 11-72 days dependent on when ethical endpoint was

met *in vivo*. These results suggest Allo-aca is effective at inhibiting LEPR downstream signalling, through ERK, in LNCaP cells *in vitro* and a weak trend *in vivo*. These results would infer factors in a more complex *in vivo* environment contribute further to the anti-tumour success of Allo-aca in mice.

Allo-aca and the tumour microenvironment: impacts on cell interactions and vascularisation

A common theme amongst canonical pathways analysed to exhibit predicted activation/inhibition with Allo-aca treatment was intracellular signalling cascades and pathways impacting cell-cell interaction/adhesion, and ultimately motility. This is evidenced in top significant canonical pathways with predicted activation/inhibition including Ephrin receptor, Rac, Rho Family GTPases and PI3K/Akt signalling (-log*P*/z= 1.8/+2.14; 1.47/+2.11; 3.02/+1.96; 2.67/-1.94, respectively) and Agrin interactions at neuromuscular junction (1.74/+2.12). Other significant canonical pathways affected in response to Allo-aca are represented in **Table1** (top 40 of 152). Similarly, MetaboAnalyst gene-centric analysis revealed four cell adhesion/motility pathways significantly impacted by Allo-aca, with Adherens junction processes one of the most significant pathways identified (**SupplFig4A**). Allo-aca may therefore impact cell adhesion, interaction and ultimately motility, processes integral to tumour growth and metastases. While subcutaneous LNCaP xenografts are highly unlikely to metastasize, as was confirmed by no metastatic growths in mice in this study, impacts of Allo-aca on cellular motility/migration were explored *in vitro*. Migration of androgen-deprived LNCaP and C4-2B cells was increased with leptin treatment and this was blunted by Allo-aca addition, especially when combined with 10nM leptin ($P<0.05$, **SupplFig4B**). These *in vitro* observations combined with knowledge of Allo-aca actions on cell interaction/adhesion *in vivo* support future testing of Allo-aca against metastatic tumour growth and spread in an *in vivo* metastasis model.

While RNAseq elucidated some potential mechanisms through which Allo-aca slowed tumour growth; clues were also inferred from tumour FFPE sections and from RNAseq data mapping to the mouse genome. Tumour sections exhibited gross changes in vascularisation, with Allo-aca-treated tumours appearing to have less blood cell infiltrate (**Fig8A**). Cell type enrichment analysis of top-expressed mouse transcripts within tumours, demonstrated significant enrichment in blood-based and/or immune cell types. When subjected to hierarchical clustering, 4 of 6 Allo-aca-treated tumours clustered as

having a greater immune cell component than other tumours; this was further confirmed by independent transcriptomic profiling by Consensus TME gene signature analysis (data not shown). Beta haemoglobin (*Hbb*) was observed in the top-15 highest expressed transcripts in 6 of 11 sequenced tumours (**SupplTable1**), and alpha haemoglobin (*Hba*) in 3 of 11 tumours. When assessed for transcript expression, *Hbb* was expressed at highest levels in the 5 Veh tumours, clustering with only 1 of 6 Allo-aca-treated tumours; suggesting greater abundance of *Hbb* in Veh (**Fig8B**). *Hba*, however, was more heterogeneous; though highest expressed *Hba* transcript *Hba-a2*, showed enrichment in 5 of 5 Veh tumours and 3 of 6 Allo-aca-treated tumours. Increased blood infiltrate was also evident at the macroscopic level (**Fig8C**). Tumour lysates probed for stimulator of angiogenesis VEGF, demonstrated decreased total VEGF ($P \leq 0.05$) and lower abundance of VEGF 35kDa isoform ($P \leq 0.01$), but unchanged VEGF 25kDa ($P=0.9$) and 10-15kDa ($P=0.3$; **Fig8E**) bands. In keeping with suppression of angiogenesis by Allo-aca, gene set signatures associated with tumour angiogenesis and VEGF signalling were negatively enriched in Allo-aca-treated tumours (vs Veh, **Fig8D**). Reduced vascularity may in part be responsible for the increased Hypoxia-inducible Factor signalling ($P<0.001$, 11/70 overlap) identified as a significant top toxicological IPA pathway in Allo-aca-treated tumours. This was supported by US/PA imaging of tumours; average sO_2 content tended to be decreased at endpoint compared to pre-treatment in Allo-aca-treated mice but not Veh ($P=0.12$, P=0.73, respectively; **Fig8F**). Similarly, contrast-enhanced US of tumours showed delayed replenishment of blood volume following microbubble destruction, indicative of lower tumour perfusion (**Fig8G**)

Furthermore, RNAseq identified 204 DE transcripts mapping to the mouse genome following Allo-aca treatment, representing host-response to Allo-aca. Top significant canonical pathways were dominated by pathways relating to immune, stress or inflammatory response, including top enriched IL-7 signalling (-log$P$=3.01 z=+2.24), (***Table2)**. Whilst other significant top pathways exhibited a metabolism- or signalling-centric theme (^**Table2**). These pathways provided a limited snapshot into the host-response to Allo-aca. Their theme suggests Allo-aca elicits an immune, stress or inflammatory response within host cells of the tumour microenvironment.

Allo-aca alters the tumour bioenergetics, lipid biosynthesis and metabolism

Lipid metabolism networks were also identified as impacted by Allo-aca treatment, consistent with leptin's fundamental role in metabolism and energy homeostasis. Expression of SREBF1, a master regulator of cholesterol and lipid synthesis (Horton et al., 2002), was increased in response to Allo-aca (vs Veh), with network interactions including (1) increased ACLY, HMGCR, FADS1, NPC1, FDFT1, G6PD expression and predicted activation of HMGCS, GYS, and (2) decreased INSIG2, FADS2 expression and predicted suppression of PEPCK (network of 28 molecules; **Fig9A**). Network changes are predicted to increase lipid and/or cholesterol synthesis in response to LEPR antagonism and suggests enhanced SREBF1 activity stem from suppressed AMPK (Li et al., 2011) **(Fig9B, C).** Western blot analysis demonstrated a trend towards lower total-AMPKα protein in Allo-aca-treated tumours (P=0.088, **Fig9D**), although abundance of phospho-AMPKα was unchanged (P=0.44), as was the ratio of Phospho:total-AMPKα (P=0.34). In keeping with altered lipid metabolism, GO gene set signatures associated with lipid synthesis and lipid transport/efflux were significantly positively and negatively enriched, respectively, within the Allo-aca-treated tumour transcriptome (**Fig9E**), while SREBP1 protein was confirmed increased (P=0.027, **Fig9F**). Altered cellular energetics are likely in part responsible for the increased Oxidative Stress (P<0.003, 9/57 overlap) identified as a significant top toxicological pathway in Allo-aca-treated tumours. Further metabolism-focused analysis (MetaboAnalyst) uncovered numerous other tumour metabolic pathways altered by Allo-aca (**Fig9G**), including riboflavin; purine; alanine, aspartate and glutamate; central carbon; pyrimidine; glycosphingolipid; glutathione; and cysteine methionine metabolism; alongside pentose phosphate pathway, TCA cycle; oxidative phosphorylation and insulin signalling changes. Cellular stresses, including accumulation of lipid species and altered energetics, are well established to trigger EIF2α signalling to attenuate global protein translation, which if sustained triggers apoptotic pathways (Wek, 2018). This is corroborated by the identification of EIF2 signalling as the most significantly deregulated pathway in tumours subjected to Allo-aca treatment (**Table1**). In combination, these data suggest Allo-aca impacts the catabolic/anabolic processes fuelling the tumour, with the potential to introduce metabolic vulnerabilities, such as lipotoxicity from increased lipid load, that could contribute to the observed tumour growth inhibition.

Ultimately our results suggest that primarily apoptotic, angiogenic and metabolic pathways are mechanistically central to the tumour growth inhibition observed with Allo-aca treatment, as summarised in **Fig10**.

Discussion:

Resistance to ADT/ATT is a leading cause of PCa mortality; consequently, therapies that target pathways employed by the tumour to evade the pressure of a low-androgen environment are therapeutically appealing. Hyperleptinemia is a well-established adaptive response to anti-androgens, with serious consequences given leptin is reported to promote PCa growth and advancement, albeit in an androgen-rich in vitro environment. Our study is the first to highlight a concomitant increase in both leptin and LEPR at the tumour level, in addition to reported hyperleptinemia, in response to ADT/ATT. We are also the first to demonstrate that pharmacological targeting of leptin signalling post-ADT is efficacious in preventing PCa growth and progression to CRPC in a preclinical model of PCa progression.

Several functional outcomes of leptin downstream signalling inherently overlap with multiple hallmarks vital for cancer growth, including altering cellular energetics, survival and death; inducing angiogenesis and migration/invasion; and promoting inflammation and an immune response (Vansaun, 2013). LEPR blockade therefore has the potential to counteract multiple pro-oncogenic pathways and combat the adaptive hyperleptinemia observed with anti-androgens. Allo-aca, a selective and potent peptide antagonist with tight LEPR binding, has previously elicited anti-tumour effects in breast cancer *in vivo* (Otvos et al., 2011); however, the impact of therapeutic LEPR blockade in PCa, and especially in an ADT environment, until now remained unknown. Like in MCF-7 breast cancer xenografts, Allo-aca inhibited growth and slowed progression in PCa xenografts, but interestingly in our study growth regression and failure for progression to CRPC were observed in ~50% of cases. Combined transcriptomic, protein and histopathological analytic approaches elucidated potential mechanistic pathways of Allo-aca's anti-tumour effect; however, were limited with tumour tissue in investigating regressing cases. In tumours with adequate tissue, enhanced cell death pathways and pro-apoptotic markers were observed with LEPR inhibition, in accordance with leptin's anti-apoptotic actions *in vitro*

(Somasundar et al., 2004), and likely contribute Allo-aca anti-tumour action. Furthermore, Allo-aca induced anti-angiogenic properties, evidenced through reduced vascularisation and lowered abundance of angiogenic driver VEGF; this is in-keeping with previous reports of leptin and LEPR antagonist action (Coroniti et al., 2016, Cao et al., 2001, Ferla et al., 2011, Gonzalez et al., 2006, Yang et al., 2016). Interestingly, enrichment in toxicological pathways of necrosis and altered hypoxia signalling were observed which could implicate an altered intratumoural environment mechanistically in the observed growth effects; however, these will be the subject of further future investigation. Despite lower vascularisation, Allo-aca appeared to boost the intratumoural immune cell recruitment, albeit in the immunocompromised Nude mouse which was essential to ensure tumour take. Interpretation of this finding is limited and warrants further investigation in an intact immune system. Though this is consistent with reports of altered immune response in transgenic non-immunocompromised animals lacking LEPR (*db/db*), where *db/db* mice exhibited increased innate immune-inflammatory factors, like macrophage function and NK cell activity, without external stimulation (Lee et al., 2010) and in those modelling atherosclerosis exhibited a regulatory T-cell immune response, protecting mice from atherosclerotic lesions (Taleb et al., 2007).

Our results also point to Allo-aca altering tumour energetics, which has the potential to limit tumour growth. AMPK signalling dysregulation in Allo-aca-treated tumours, predicted by gene set enrichment analyses, and indicated by lowered AMPK protein, suggests impacted intratumoural ATP balance. This is consistent with the observed increase in lipid synthesis pathways by functional enrichment analysis and lipogenic mediator SREBP1 protein; suggesting the potential for higher tumour lipids to suppress AMPK protein (Viollet et al., 2010). Increased lipid load within tumour cells may induce lipotoxicity, which could contribute to enrichment of pathways for oxidative stress observed in RNAseq analysis (Hauck and Bernlohr, 2016), potentially impacting tumour cell survival. Likewise, lipid-induced ER stress may contribute to the top canonical pathway affected in Allo-aca-treated tumours, EIF2 signalling (Han and Kaufman, 2016, Wek, 2018), alluding to reduced protein translation, which may also play a role in tumour shrinkage. While Allo-aca showed clear efficacy *in vivo*, *in vitro* results in multiple androgen-deprived AR-positive/androgen-sensitive cell lines were less clear-cut. The *in vivo* data discussed above highlight the importance of Allo-aca eliciting multiple anti-cancer effects not only

within the tumour cells, but on the several cell types expressing the LEPR, that make up the tumour microenvironment, including, but not limited to, immune cells, adipocytes and vasculature (Tartaglia et al., 1995, Procaccini et al., 2017).

This study is the first rigorous investigation of the impacts of leptin, and inhibition of leptin signalling, in androgen targeted PCa. While we elucidate potential mechanisms (**Figure 10**) for the anti-tumour efficacy of LEPR antagonism, guided by *in vitro* PCa monoculture and *in vivo* prostate tumour xenografts in immunocompromised mice, limitations exist inherent to these models as discussed throughout. In future *in vitro* studies, LEP ± LEPR knockdown alongside leptin and Allo-aca treatment in mono and co-culture systems could be used to further dissect the complex endocrine interplay of leptin signalling and its blockade across cell types, e.g., PCa endothelial, adipocytes, PCa cell lines, which are not observed in monoculture alone. Systemic impacts of Allo-aca blockade in combination with ATTs should be explored in both animal models with an intact immune system and those engineered to carry tumour-specific LEPR knockdown to further reveal the effects of Allo-aca specific to the tumour or its microenvironment. These additional studies, beyond the scope of the current investigation, are expected to provide further insight into this understudied complex hormone signalling system in PCa with endocrine, paracrine and potential autocrine implications. Based on the complex role of leptin in several cancer hallmark pathways and a hyper-leptin signalling environment in PCa in an ATT environment, this study harnessed leptin signalling blockade, using selective LEPR antagonism, to inhibit multiple cancer-inducing pathways. This is the first report in a PCa xenograft combining LEPR antagonist with ADT, where Allo-aca significantly reduced tumour burden and delayed progression to CRPC. Allo-aca's *in vivo* efficacy may be related to apoptosis, increased immune response, reduced tumour vascularity, induced stress through altered energetics and lipotoxicity. This study suggests that novel leptin signalling blockade strategies should be investigated in conjunction with ADT/ATTs as a novel treatment strategy for progression to CRPC.

Acknowledgements:

The authors thank Ms Ellca Ratther for technical assistance with ELISA assays and Dr Brian WC Tse, Translational Research Institute Preclinical Imaging Facility, for technical assistance with US/PA imaging.

Funding Sources:

This work is supported by the Australian Government Department of Health; and the Movember Foundation and the Prostate Cancer Foundation of Australia through a Movember Revolutionary Team Award (LKP, AR, MLL, NB, CCN) and the Princess Alexandra Hospital Research Foundation "It's a Blokes Thing" grant. The Translational Research Institute is supported by a grant from the Australian Government. JDW is an NHMRC Principal Research Fellow (APP1117483). Research at The Florey Institute of Neuroscience and Mental Health is supported by the Victorian Government Operational Infrastructure Support Program.

Conflicts of Interest:

The authors declare no potential conflicts of interest.

References:

BANKHEAD, P., LOUGHREY, M. B., FERNANDEZ, J. A., DOMBROWSKI, Y., MCART, D. G., DUNNE, P. D., MCQUAID, S., GRAY, R. T., MURRAY, L. J., COLEMAN, H. G., et al. 2017. QuPath: Open source software for digital pathology image analysis. *Sci Rep,* 7**,** 16878.

BASARIA, S., MULLER, D. C., CARDUCCI, M. A., EGAN, J. & DOBS, A. S. 2006. Hyperglycemia and insulin resistance in men with prostate carcinoma who receive androgen-deprivation therapy. *Cancer,* 106**,** 581-8.

CAO, R., BRAKENHIELM, E., WAHLESTEDT, C., THYBERG, J. & CAO, Y. 2001. Leptin induces vascular permeability and synergistically stimulates angiogenesis with FGF-2 and VEGF. 98**,** 6390-6395.

CORONITI, R., FARIO, R., NUNO, D. J., OTVOS, L., SCOLARO, L. & SURMACZ, E. 2016. Designer Leptin Receptor Antagonist Allo-aca Inhibits VEGF Effects in Ophthalmic Neoangiogenesis Models. *Front Mol Biosci,* 3**,** 67.

DE MARINIS, L., BIANCHI, A., MANCINI, A., GENTILELLA, R., PERRELLI, M., GIAMPIETRO, A., PORCELLI, T., TILARO, L., FUSCO, A., VALLE, D., et al. 2004. Growth Hormone Secretion and Leptin in Morbid Obesity before and after Biliopancreatic Diversion: Relationships with Insulin and Body Composition. *The Journal of Clinical Endocrinology & Metabolism,* 89**,** 174-180.

ETTINGER, S. L., SOBEL, R., WHITMORE, T. G., AKBARI, M., BRADLEY, D. R., GLEAVE, M. E. & NELSON, C. C. 2004. Dysregulation of sterol response element-binding proteins and downstream

effectors in prostate cancer during progression to androgen independence. *Cancer Res,* 64**,** 2212-21.

FARIS, J. E. & SMITH, M. R. 2010. Metabolic sequelae associated with androgen deprivation therapy for prostate cancer. *Current opinion in endocrinology, diabetes, and obesity,* 17**,** 240-246.

FERLA, R., BONOMI, M., OTVOS, L. & SURMACZ, E. 2011. Glioblastoma-derived Leptin Induces Tube Formation and Growth of Endothelial Cells: Comparison with VEGF Effects. *BMC Cancer,* 11**,** 303.

FRANKENBERRY, K. A., SOMASUNDAR, P., MCFADDEN, D. W. & VONA-DAVIS, L. C. 2004. Leptin induces cell migration and the expression of growth factors in human prostate cancer cells. *Am J Surg,* 188**,** 560-5.

GONZALEZ, R. R., CHERFILS, S., ESCOBAR, M., YOO, J. H., CARINO, C., STYER, A. K., SULLIVAN, B. T., SAKAMOTO, H., OLAWAIYE, A., SERIKAWA, T., et al. 2006. Leptin Signaling Promotes the Growth of Mammary Tumors and Increases the Expression of Vascular Endothelial Growth Factor (VEGF) and Its Receptor Type Two (VEGF-R2) *. *Journal of Biological Chemistry,* 281**,** 26320-26328.

GORRAB, A., PAGANO, A., AYED, K., CHEBIL, M., DEROUICHE, A., KOVACIC, H. & GATI, A. 2020. Leptin Promotes Prostate Cancer Proliferation and Migration by Stimulating STAT3 Pathway. *Nutr Cancer***,** 1-11.

HABIB, C. N., AL-ABD, A. M., TOLBA, M. F., KHALIFA, A. E., KHEDR, A., MOSLI, H. A. & ABDEL-NAIM, A. B. 2015. Leptin influences estrogen metabolism and accelerates prostate cell proliferation. *Life Sciences,* 121**,** 10-15.

HAN, J. & KAUFMAN, R. J. 2016. The role of ER stress in lipid metabolism and lipotoxicity. *Journal of Lipid Research,* 57**,** 1329-1338.

HARRIS, W. P., MOSTAGHEL, E. A., NELSON, P. S. & MONTGOMERY, B. 2009. Androgen deprivation therapy: progress in understanding mechanisms of resistance and optimizing androgen depletion. *Nature clinical practice. Urology,* 6**,** 76-85.

HAUCK, A. K. & BERNLOHR, D. A. 2016. Oxidative stress and lipotoxicity. *Journal of Lipid Research,* 57**,** 1976-1986.

HORTON, J. D., GOLDSTEIN, J. L. & BROWN, M. S. 2002. SREBPs: activators of the complete program of cholesterol and fatty acid synthesis in the liver. *J Clin Invest,* 109**,** 1125-31.

JENKS, M. Z., FAIRFIELD, H. E., JOHNSON, E. C., MORRISON, R. F. & MUDAY, G. K. 2017. Sex Steroid Hormones Regulate Leptin Transcript Accumulation and Protein Secretion in 3T3-L1 Cells. *Scientific reports,* 7**,** 8232-8232.

LEE, S.-E., JANG, I.-S., PARK, J.-S., LEE, J.-H., LEE, S.-Y., BAEK, S.-Y., LEE, S.-H. & LEE, H. 2010. Systemic immunity of obese-diabetes model (db/db) mice. *Molecular & Cellular Toxicology,* 6**,** 143-149.

LI, Y., XU, S., MIHAYLOVA, M. M., ZHENG, B., HOU, X., JIANG, B., PARK, O., LUO, Z., LEFAI, E., SHYY, J. Y., et al. 2011. AMPK phosphorylates and inhibits SREBP activity to attenuate hepatic steatosis and atherosclerosis in diet-induced insulin-resistant mice. *Cell Metab,* 13**,** 376-388.

LOCKE, J. A., GUNS, E. S., LUBIK, A. A., ADOMAT, H. H., HENDY, S. C., WOOD, C. A., ETTINGER, S. L., GLEAVE, M. E. & NELSON, C. C. 2008. Androgen levels increase by intratumoral de novo steroidogenesis during progression of castration-resistant prostate cancer. *Cancer Res,* 68**,** 6407-15.

MAUGHAM, M., THOMAS, P., CRISP, G., PHILP, L., SHAH, E., HERINGTON, A., CHEN, C., GREGORY, L., NELSON, C., SEIM, I., et al. 2017. Insights from engraftable immunodeficient mouse models of hyperinsulinaemia. 7**,** Article number: 491 1-10.

NODA, T., KIKUGAWA, T., TANJI, N., MIURA, N., ASAI, S., HIGASHIYAMA, S. & YOKOYAMA, M. 2015. Longterm exposure to leptin enhances the growth of prostate cancer cells. *Int J Oncol,* 46**,** 1535-42.

OTVOS, L., JR., KOVALSZKY, I., RIOLFI, M., FERLA, R., OLAH, J., SZTODOLA, A., NAMA, K., MOLINO, A., PIUBELLO, Q., WADE, J. D., et al. 2011. Efficacy of a leptin receptor antagonist peptide in a mouse model of triple-negative breast cancer. *Eur J Cancer,* 47**,** 1578-84.

OTVOS, L., KNAPPE, D., HOFFMANN, R., KOVALSZKY, I., OLAH, J., HEWITSON, T. D., STAWIKOWSKA, R., STAWIKOWSKI, M., CUDIC, P., LIN, F., et al. 2014. Development of second generation peptides modulating cellular adiponectin receptor responses. *Frontiers in Chemistry,* 2**,** 93.

PHILP, L. K., DAY, T. K., BUTLER, M. S., LAVEN-LAW, G., JINDAL, S., HICKEY, T. E., SCHER, H. I., BUTLER, L. M. & TILLEY, W. D. 2016. Small Glutamine-Rich Tetratricopeptide Repeat-Containing Protein Alpha (SGTA) Ablation Limits Offspring Viability and Growth in Mice. *Sci Rep,* 6**,** 28950.

PHILP, L. K., MUHLHAUSLER, B. S., JANOVSKA, A., WITTERT, G. A., DUFFIELD, J. A. & MCMILLEN, I. C. 2008. Maternal overnutrition suppresses the phosphorylation of 5'-AMP-activated protein kinase in liver, but not skeletal muscle, in the fetal and neonatal sheep. *Am J Physiol Regul Integr Comp Physiol,* 295**,** R1982-90.

PHILP, L. K., ROCKSTROH, A., LEHMAN, M., SADOWSKI, M. C., BARTONICEK, N., WADE, J. D., JR, L. O. & NELSON, C. C. 2020. Adiponectin receptor activation inhibits prostate cancer xenograft growth *Endocrine-Related Cancer,* Accepted 1 Oct 2020**,** ERC-20-0297.

PROCACCINI, C., LA ROCCA, C., CARBONE, F., DE ROSA, V., GALGANI, M. & MATARESE, G. 2017. Leptin as immune mediator: Interaction between neuroendocrine and immune system. *Developmental & Comparative Immunology,* 66**,** 120-129.

RAMOS-MONTOYA, A., LAMB, A. D., RUSSELL, R., CARROLL, T., JURMEISTER, S., GALEANO-DALMAU, N., MASSIE, C. E., BOREN, J., BON, H., THEODOROU, V., et al. 2014. HES6 drives a critical AR transcriptional programme to induce castration-resistant prostate cancer through activation of an E2F1-mediated cell cycle network. *EMBO Mol Med,* 6**,** 651-61.

SADOWSKI, M. C., POUWER, R. H., GUNTER, J. H., LUBIK, A. A., QUINN, R. J. & NELSON, C. C. 2014. The fatty acid synthase inhibitor triclosan: repurposing an anti-microbial agent for targeting prostate cancer. *Oncotarget,* 5**,** 9362-81.

SARMENTO-CABRAL, A., F, L. L. & LUQUE, R. M. 2017. Adipokines and Their Receptors Are Widely Expressed and Distinctly Regulated by the Metabolic Environment in the Prostate of Male Mice: Direct Role Under Normal and Tumoral Conditions. *Endocrinology,* 158**,** 3540-3552.

SHARIFI, N. 2013. Mechanisms of androgen receptor activation in castration-resistant prostate cancer. *Endocrinology,* 154**,** 4010-4017.

SHOEMAKER, J. E., LOPES, T. J. S., GHOSH, S., MATSUOKA, Y., KAWAOKA, Y. & KITANO, H. 2012. CTen: a web-based platform for identifying enriched cell types from heterogeneous microarray data. *BMC Genomics,* 13**,** 460.

SIEH, S., TAUBENBERGER, A. V., RIZZI, S. C., SADOWSKI, M., LEHMAN, M. L., ROCKSTROH, A., AN, J., CLEMENTS, J. A., NELSON, C. C. & HUTMACHER, D. W. 2012. Phenotypic characterization of prostate cancer LNCaP cells cultured within a bioengineered microenvironment. *PLoS One,* 7**,** e40217.

SOMASUNDAR, P., FRANKENBERRY, K. A., SKINNER, H., VEDULA, G., MCFADDEN, D. W., RIGGS, D., JACKSON, B., VANGILDER, R., HILEMAN, S. M. & VONA-DAVIS, L. C. 2004. Prostate cancer cell proliferation is influenced by leptin. *J Surg Res,* 118**,** 71-82.

SOMASUNDAR, P., YU, A. K., VONA-DAVIS, L. & MCFADDEN, D. W. 2003. Differential effects of leptin on cancer in vitro. *J Surg Res,* 113**,** 50-5.

TALEB, S., HERBIN, O., AIT-OUFELLA, H., VERRETH, W., GOURDY, P., BARATEAU, V., MERVAL, R., ESPOSITO, B., CLEMENT, K., HOLVOET, P., et al. 2007. Defective leptin/leptin receptor signaling improves regulatory T cell immune response and protects mice from atherosclerosis. *Arterioscler Thromb Vasc Biol,* 27**,** 2691-8.

TARTAGLIA, L. A., DEMBSKI, M., WENG, X., DENG, N., CULPEPPER, J., DEVOS, R., RICHARDS, G. J., CAMPFIELD, L. A., CLARK, F. T., DEEDS, J., et al. 1995. Identification and expression cloning of a leptin receptor, OB-R. *Cell,* 83**,** 1263-1271.

TEVZ, G., MCGRATH, S., DEMETER, R., MAGRINI, V., JEET, V., ROCKSTROH, A., MCPHERSON, S., LAI, J., BARTONICEK, N., AN, J., et al. 2016. Identification of a novel fusion transcript between human relaxin-1 (RLN1) and human relaxin-2 (RLN2) in prostate cancer. *Mol Cell Endocrinol,* 420**,** 159-68.

TILKI, D., SCHAEFFER, E. M. & EVANS, C. P. 2016. Understanding Mechanisms of Resistance in Metastatic Castration-resistant Prostate Cancer: The Role of the Androgen Receptor. *European Urology Focus,* 2**,** 499-505.

TOUSIGNANT, K. D., ROCKSTROH, A., TAHERIAN FARD, A., LEHMAN, M. L., WANG, C., MCPHERSON, S. J., PHILP, L. K., BARTONICEK, N., DINGER, M. E., NELSON, C. C., et al. 2019. Lipid Uptake Is an Androgen-Enhanced Lipid Supply Pathway Associated with Prostate Cancer Disease Progression and Bone Metastasis. *Molecular Cancer Research*.

VANSAUN, M. N. 2013. Molecular pathways: adiponectin and leptin signaling in cancer. *Clin Cancer Res,* 19**,** 1926-32.

VIOLLET, B., HORMAN, S., LECLERC, J., LANTIER, L., FORETZ, M., BILLAUD, M., GIRI, S. & ANDREELLI, F. 2010. AMPK inhibition in health and disease. *Critical reviews in biochemistry and molecular biology,* 45**,** 276-295.

WANG, H., BURKE, L. J., PATEL, J., TSE, B. W. C., BRIDLE, K. R., COGGER, V. C., LI, X., LIU, X., YANG, H., CRAWFORD, D. H. G., et al. 2020. Imaging-based vascular-related biomarkers for early detection of acetaminophen-induced liver injury. *Theranostics,* 10**,** 6715-6727.

WEK, R. C. 2018. Role of eIF2α Kinases in Translational Control and Adaptation to Cellular Stress. *Cold Spring Harbor perspectives in biology,* 10**,** a032870.

XU, C. J., DONG, L. L., KANG, X. L., LI, Z. M. & ZHANG, H. Y. 2020. Leptin promotes proliferation and inhibits apoptosis of prostate cancer cells by regulating ERK1/2 signaling pathway. *Eur Rev Med Pharmacol Sci,* 24**,** 8341-8348.

YANG, W.-H., CHANG, A.-C., WANG, S.-W., WANG, S.-J., CHANG, Y.-S., CHANG, T.-M., HSU, S.-K., FONG, Y.-C. & TANG, C.-H. 2016. Leptin promotes VEGF-C production and induces lymphangiogenesis by suppressing miR-27b in human chondrosarcoma cells. *Scientific Reports,* 6**,** 28647.

ZHU, Z., SHI, M., HU, W., ESTRELLA, H., ENGEBRETSEN, J., NICHOLS, T., BRIERE, D., HOSEA, N., LOS, G., REJTO, P. A., et al. 2012. Dose-dependent effects of small-molecule antagonists on the genomic landscape of androgen receptor binding. *BMC Genomics,* 13**,** 355.

Figure Legends:

Figure 1 (A-D). Tumour leptin (*LEP*) and leptin receptor (*LEPR*) expression increases with PCa progression and in treatment resistant disease in patient samples. (A-B) *LEP* and *LEPR* expression evaluated in PCa patient samples using the Oncomine platform (transcriptomic and genomic datasets). ata represents **(A)** increased *LEP* expression in the Arredouani, Glinksy, Taylor 3 and Nanni patient datasets for primary vs non-malignant prostate, increasing Gleason score, metastatic vs localized PCa, recurrence vs non-recurrent at 1 yrs, respectively; and **(B)** increased *LEPR* expression in the Liu, La pointe, Chandran and Glinksy patient datasets for primary vs non-malignant prostate, increasing Gleason score, metastatic vs localized PCa, and recurrence vs non-recurrent at 1 yrs, respectively. Significant (**P*<0.05) and trending (^{t}P=0.055-0.07) *P*-values indicated. **(C)** *LEPR* expression evaluated in the Rajan dataset in PCa biopsies profiled transcriptomically pre- and post-ADT (*P*<0.01). **(D)** *LEPR* expression evaluated in metastases in the Abida dataset, presented according to primary or metastatic tissue biopsy site and stratified according to NEPC score by color and neuroendocrine features by symbol, at localized or metastatic sites.

Figure 2 (A-G). Leptin receptor (*LEPR*) expression increases in cell lines subjected to androgen withdrawal *in vitro* and *in vivo*. (A) *LEPR* mRNA expression (by microarray) in LNCaP, DUCaP, VCaP PCa cell lines in normal growth media (FBS) or androgen deplete (Charcoal stripped serum, CSS) and replete (CSS + DHT) conditions. Significant: **P*≤0.05. **(B)** *LEPR* mRNA expression (by RNAseq) in LNCaP cells in androgen deplete media (CSS) or androgen replete media (+D) ± androgen targeted (+ENZ) therapy. **P*≤0.05. **(C)** *LEPR* mRNA expression (by RNAseq) in shAR LNCaP cells grown in androgen deplete media (CSS) ±treatment with doxycycline (Dox) for knockdown induction (shNT, shAR) and DHT for androgen replete conditions (upper panel). *AR* mRNA expression under Dox-induction demonstrates successful AR knockdown by inducible shAR (lower panel, #*P*≤0.05 indicates validated knockdown in +Dox vs no Dox). Significant: **P*≤0.05. **(D)** *LEPR* mRNA expression (by microarray) in an LNCaP prostate cancer progression xenograft model in mice. Xenografts were harvested from intact mice or mice that underwent castration with tumors collected at PSA progression

points (Regression (REGR); Nadir, Recurrence (RECUR) or Castrate Resistance (CRPC)) . Significant: *$P \leq 0.05$, vs Intact; trend $^{T}P \leq 0.1$ vs CRPC. Progression of serum PSA across model time points indicated by schematic below. **(E)** Two independent experiments validating increased *LEPR* mRNA expression in androgen deplete conditions by qRT-PCR. Relative *LEPR* mRNA in LNCaP cells subjected to acute androgen deplete (CSS) or replete (CSS + DHT) conditions (n=1, mean ± SD) (left panel). Relative *LEPR* mRNA expression in LNCaP cells subjected to either normal growth media (FBS) (d0) or to chronic androgen deplete (CSS) conditions over up to 8 days. At day 8, cells were either maintained in androgen deplete (CSS) conditions or androgens were re-introduced (+DHT) for up to 6 days (n=1, mean ± SD) (right panel). **(F)** Human LEPR protein abundance measured in LNCaP PCa cell lysates relative to γ-tubulin loading control; densitometry was performed to quantify abundance from membrane total LEPR and background corrected. Cells were pretreated with ADT (CSS) for 48h and then subjected to 48h leptin (L, 10 nM) ± Allo-aca (A, 100 nM). Western blot, n=2; Lad = prestained protein ladder. Significant: *$P \leq 0.05$, vs FBS. (G) *LEPR* mRNA expression (by RNAseq) in LNCaP cells subjected to 2d androgen deplete media (CSS) or androgen rich media (FBS), followed by 48h (L, 10 nM) ± Allo-aca (A, 100 nM) treatment. Significant: *$P \leq 0.05$, vs FBS.

Figure 3 (A-C). Androgens regulate the expression of LEP and LEPR. (A) AR ChIPseq peak enrichment analysis of LEP and LEPR in the Ramos-Montoya data set of LNCaP cells treated with bicalutamide (BIC) compared with vehicle control. The number of peaks is highlighted by the bubble size and the enrichment score by the gray scale. **(B)** Regulatory potential (RP) score of AR analysed across datasets within the Cistrome database using AR ChIPseq peaks enriched within 1kb and 10kb of LEPR transcription start. Graph demonstrating AR RP score across samples compared to that of other transcription factors (y-axis) as a promoter-type transcription factor, within 1kb of LEPR transcription start. Heatmap detailing AR RP score across samples as an enhancer-type transcription factor, within 10kb of LEPR transcription start. **(C).** AR ChIPseq peaks displayed within and surrounding LEPR in the Zhu data set of VCaP cells and changes associated with small compound AR antagonist treatment (Compound 26, Compound 30) compared vehicle, androgen R1881 alone.

Figure 4 (A-H). Efficacious effects of Allo-aca in preventing tumour progression in LNCaP xenograft progression model in castrate Nude mice. Impact of Allo-aca on tumor xenograft **(A)** doubling time (^in cohort growth inhibition cohort n=5 Allo); **(B)** endpoint volume and **(C)** endpoint mass. **(D)** Serum PSA at endpoint and **(E)** time to PSA recurrence post-castration (^in cohort growth inhibition cohort n=5 Allo). **(F)** Time to ethical endpoint. **(G)** Progression to ethical endpoint by survival analysis. **(H)** Time to castration. Statistics: versus Veh, significant *$P \leq 0.05$ and trending ^{t} P=0.055-0.10; N/S, not significant; P-values indicated. n=11 vehicle (Veh), n=10 Allo-aca (Allo) unless indicated.

Figure 5 (A-J). Allo-aca had no impact on normal physiology and was well-tolerated in the LNCaP xenograft progression model in castrate Nude mice. Impact of Allo-aca (Allo) on mouse **(A)** body weight at endpoint; **(B)** absolute organ weight; **(C)** absolute serum leptin, compared to Vehicle (Veh). Assessment of correlation between serum leptin and **(D)** time on treatment, and **(E)** serum PSA in all mice. Impact of Allo on **(F)** serum leptin corrected for time on treatment, and **(G)** absolute serum adiponectin, compared to Veh. Assessment of correlation between serum adiponectin and **(H)** time on treatment, and **(I)** serum PSA in all mice. Statistics: versus Veh, significant *$P \leq 0.05$ and trending ^{t} P=0.055-0.10; P-values indicated; N/S, not significant. n=11 vehicle (Veh), n=10 Allo-aca (Allo) unless indicated. **(j)** Allo-aca has no effect on tissue pathology. Organ pathology by hematoxylin and eosin staining of heart, genitourinary (GU) tract (prostate and seminal vesicles indicated), brown (BAT) and white (WAT) adipose tissue, liver, kidney, pancreas, lymph node, muscle (quads, quadricep), spleen, brain and lung (scale bar = 100μm).

Figure 6 (A-F). Allo-aca impacts tumor xenograft apoptotic processes..) Pathway of apoptosis signalling, from IPA analysis of DE transcripts following tumor xenograft RNAseq. This map shows that apoptosis is a significantly affected canonical pathway induced by Allo-aca treatment. **(B)** Heatmap showing the expression of pro- and anti-apoptotic genes across tumor samples subjected to RNAseq. **(C)** Significant enrichment of Curtois, 'GO' and Reactome molecular signatures within the Allo-aca transcriptomic dataset (mapped to human) related to apoptosis and cellular senescence. Enr =

enrichment. Statistics: $^{*}P<0.05$, trend $^{T}P=0.055$-0.10, *P*-values indicated. **(D)** Protein abundance of apoptotic marker, cleaved caspase 3 (active apoptosis) and pro-caspase 3, relative to vinculin loading control in tumour xenograft lysates. Densitometry was performed to quantify abundance from membrane; cleaved caspase detection of bands at ~17, 19 kDa and pro-caspase at ~35kDa was expressed relative to vinculin (~125kDa) and background corrected. Western blot, n=11 Veh, n=5 Allo; Lad = prestained protein ladder. Statistics: $^{*}P<0.05$, *P*-values indicated. **(E)** Cell viability-associated pathways detected as significantly altered by Z-score and -logP according to IPA analysis. **(F)** Representative images of 3 tumors probed for Ki-67 proliferative marker by immunohistochemistry. Ki-67 positive cells are stained brown (DAB), light counterstain with hematoxylin (scale bar =50μm). Minus primary antibody (-1°) matching area for Ki-67 staining provided above Ki-67 stained images to show specificity of Ki-67 staining. Ki-67 score, based on intensity and positivity, derived from tumor sections probed by immunohistochemistry with antibody raised against human Ki-67. Statistics, not significant (N/S); Veh (vehicle), n=10, Allo-aca (Allo) n=7**.** Expression of human Ki-67 gene, *MIK67*, in RNAseq from Allo-aca and Vehicle-treated tumors (fpkm); Statistics, not significant (N/S).

Figure 7 (A-F). Effect of leptin and Allo-aca on androgen-deprived PCa cell growth *in vitro*. (A) Change in confluence following 72h treatment with leptin (0, 2.5, 10, 20 nM) ± Allo-aca (0, 1, 10, 100nM) in androgen-deprived conditions in LNCaP, LAPC4, DuCaP, and C4-2B cells that had been pre-subjected to 48h androgen deprivation (media supplemented with charcoal stripped serum (CSS) or serum free media supplemented with BSA). Confluence 72h post-drug treatment, measured by IncuCyte, was represented relative to pretreatment confluence at time 0h. n=3; N/S, not significant. **(B)** Change in confluence following 48h treatment with leptin (0, 10, 20 nM) ± Allo-aca (0, 10, 100nM) in FBS ± Enzalutamide conditions in LNCaP cells that had been pre-subjected to 48h ATT (FBS media supplemented with Enzalutamide (10μM)). Confluence 48h post-drug treatment, measured by IncuCyte, was represented relative to pretreatment confluence at time 0h. n=1; N/S, not significant. **(C)** Cell number was assessed by DNA content using CyQuant (n=3) and expressed relative to pre-treatment values. Data represent LNCaP, DuCaP, LAPC4 and C4-2B cell lines exposed

to 72h treatment with leptin (0, 0.5, 2.5, 5, 10, 20, 50 nM) ± Allo-aca (0, 1, 10, 100nM) in androgen-deprived conditions (CSS), with cells subjected to 48h androgen deprivation (media supplemented with charcoal stripped serum (CSS) prior to drug treatment. * $P<0.05$, vs CSS; # $P<0.05$, vs leptin dose alone; t trend, $P<0.1$. **(D)** Heatmap showing significant changes to ERK/MAPK signalling genes across tumor samples subjected to RNAseq. **(E)** Protein abundance of phospho (P-) ERK and total ERK, relative to vinculin loading control in tumor xenograft lysates. Densitometry was performed to quantify abundance from membrane; ERK detection of bands at 44/42 kDa (total, red channel; P-, green channel) was expressed relative to vinculin (~125kDa) and background corrected. Western blot, n=11 Veh, n=5 Allo; Lad = prestained protein ladder. Statistics: trend ^{t} $P=0.055$-0.10, P-values indicated; N/S, not significant. **(F)** Alpha-screen assessment of ERK signaling in LNCaP cells treated with leptin (20nM) ± Allo-aca (100nM) compared to controls (DMSO, U0126 (selective MEK1, 2 inhibitor, to inhibit the Ras/Raf/MEK/ERK signalling pathway)). Statistics: * $P<0.05$, vs DMSO; # $P<0.05$, vs leptin dose alone.

Figure 8 (A-G). Effect of Allo-aca on tumor xenograft phenotype and host microenvironment. **(A)** Tumor pathology by hematoxylin and eosin staining (scale bar: whole tumor = 1mm; magnified view =100μm); **(B)** Abundance of mouse transcripts for hemoglobin (beta (*Hbb*); alpha (*Hba*)) across tumor samples subjected to RNAseq; **(C)** Representative endpoint images showing Allo-aca altered tumor xenograft phenotype compared to Vehicle (ruler ticks at 1mm intervals); **(D)** Significant enrichment of molecular signatures within the Allo-aca transcriptomic dataset (mapped to human) related to angiogenesis. **(E)** Human VEGF protein abundance measured in tumor xenograft lysates relative to vinculin loading control; densitometry was performed to quantify abundance from membrane VEGF detection of bands at 35kDa, 25 kDa and at ~ 10,15 kDa and the sum of all protein (total). Vinculin (~125kDa) was used as a loading control. Lad = prestained protein ladder. Statistics: versus Veh, significant *$P\leq0.05$, **$P<0.01$. RNAseq, n=6 Allo-aca (Allo), n=5 Vehicle (Veh); Western blot, n=11 Veh, n=4 Allo. (F) Average sO_2 content at endpoint (compared to pretreatment)

by live longitudinal PA spectral imaging of tumours, n=9 Allo, n=11 Veh; trend ^{t}P=0.12. (G) Perfusion in Veh and Allo-aca endpoint tumours (n=1) demonstrated using US contrast agent replenishment (transit time (TT) (s), colour scale X = maximum TT for that image).

Figure 9(A-G). Effect of Allo-aca on cholesterol and lipid synthesis, and metabolic networks, in tumor xenografts derived from gene function analysis of RNAseq data using IPA and MetaboAnalyst. (A) "Lipid Metabolism, Small Molecule Biochemistry, Vitamin and Mineral Metabolism" identified as a key network significantly affected by Allo-aca (as compared to Vehicle); featuring upregulation of Master lipogenic regulator, SREBF1 and altered expression of several lipid and glucose metabolism enzymes. **(B)** Predicted AMPK suppression within the **"**Lipid Metabolism, Small Molecule Biochemistry, Vitamin and Mineral Metabolism" network; a potential mechanism for enhanced SREBF1 expression and predicted activity. **(C)** Heatmap representing altered expression of genes associated with lipid metabolism and AMPK signaling pathways from RNAseq analysis across Allo-aca-treated tumors, vs Vehicle (Veh) control; as identified in IPA analysis shown in (A) and (B). (A-C) Statistics: significant adjusted P-value $P \leq 0.05$, fold change (FC) cut off > +1.5, <-1.5. RNAseq, n=6 Allo-aca (Allo), n=5 Veh. Legend – red = upregulated, green = downregulated, orange = predicted upregulated based on pathway activation, blue = predicted downregulated based on pathway activation. **(D)** Protein abundance of total AMPKα and phospho (P-) AMPKα, relative to vinculin loading control in tumor xenograft lysates. Densitometry was performed to quantify abundance from membrane; AMPK detection of bands at 62kDa (total, red channel; P-, green channel) was expressed relative to vinculin (~117kDa) and background corrected. Western blot, n=11 Veh, n=4 Allo; Lad = prestained protein ladder. Statistics: trend ^{t}P=0.055-0.10, *P*-values indicated; N/S, not significant. **(E)** Significant enrichment of several 'GO' molecular signatures within the Allo-aca transcriptomic dataset (mapped to human) related to lipid metabolism and transport. Listed pathway; enrichment score. Statistics: *P<0.05, trend *T* P=0.055-0.10. **(F)** Protein abundance of SREBP1, relative to vinculin loading control in tumor xenograft lysates. Densitometry was performed as above 122kDa SREBP1 was expressed relative to vinculin (~117kDa) and background corrected. Western blot,

n=11 Veh, n=5 Allo. Statistics: *P*-values indicated. **(G)** Other metabolic pathways (not lipid centric) that were also observed to be significantly enriched in MetaboAnalyst analyses of the Allo-aca-treated tumour transcriptome. Highlighted metabolism (met.) pathways are indicated by numbers alongside green circled nodes on the graph and details seen in the corresponding table. Node size corresponds to impact score while node colour corresponds to -log10*P* significance.

Figure 10. Schematic of leptin impacts on tumor xenograft phenotype and microenvironment and potential mechanisms highlighted to underlie anti-tumour efficacy of leptin signalling blockade by Allo-aca. Our and previous research supports leptin eliciting effects on the tumour and its microenvironment that are supportive of tumour growth and aggressiveness. This study has informed potential mechanisms of the growth limiting actions of Allo-aca on prostate tumours, which include induction of apoptosis, decreased tumour angiogenesis, altered tumour immune/inflammatory environment and rewired metabolism.

Suppl Fig1. Human transcripts (tumour-specific) from Allo-aca (Allo) and Vehicle (Veh) treated tumors cluster separately in PCA plots of normalized CPM of human transcripts, COA plots of normalized CPM of human transcripts and PCA plots of normalized logCPM of differentially expressed (DE) human transcripts. 1448 DE human transcripts were observed with Allo-aca treatment.

Suppl Fig2(A-E). Allo-aca efficacy in LNCaP xenograft progression model in castrate Nude mice. Progression over time of **(A)** tumor xenograft volume from day 0 and **(B)** serum PSA from castration. Regression over time of **(C)** tumor volume and **(D)** serum PSA in the Allo regression cohort n=5). **(E)** Correlation of endpoint tumor PSA and volume. Cx = castration.

Suppl Fig3. Impact of leptin and Allo-aca on LNCaP cell LEPR protein. Representative images of LEPR (green) protein by immunofluorescence in LNCaP cells treated with acute leptin (10 nM) and Allo-aca (100 nM) *in vitro* under androgen deplete (CSS) or rich (FBS) conditions. Graphically

represented as overall LEPR intensity of cells as calculated by Cell Profiler analysis. Statistics: $^{**}P \leq 0.01$, $^{***}P \leq 0.001$ vs vehicle; $^{\#}P \leq 0.05$, $^{\#\#\#}P \leq 0.001$ vs leptin alone in that condition.

Suppl Figure 4 (A-B). Effect of Allo-aca on tumor xenograft phenotype and migration. (A) MetaboAnalyst gene-centric pathway analysis showing significant enrichment of pathways associated with cell adhesion/motility in Allo-aca treated tumours. Analysis was performed on differentially expressed transcripts mapping to the human genome. Pathways are indicated by numbers alongside green circled nodes on the graph and details seen in the corresponding table. Node size corresponds to impact score while node colour corresponds to -log10P significance. **(B)** Effect of leptin and Allo-aca on androgen-deprived PCa cell transwell migration in vitro. Relative number of migrating LNCaP and C4-2B cells following androgen-deprivation and treatment with leptin doses (0, 2.5, 10 nM), and leptin doses + Allo-aca (1, 10, 100nM); expressed relative to ADT vehicle control. n=3; Statistics: *P<0.05, ***P<0.001, ****P<0.0001, vs ADT vehicle; tP=0.055-0.10, #P<0.05, ##P<0.01, ###P<0.001, vs leptin dose alone.

Table 1. Top 40 significantly represented canonical pathways, as assessed by IPA using transcripts mapping only to the human genome, in Allo-aca-treated tumour xenografts (as compared to Veh), based on –log(*P*).

Ingenuity Canonical Pathways	-log(*P*)	z-score
EIF2 Signalling	6.78	1.15
Epithelial Adherens Junction Signalling	5.32	N/A
Molecular Mechanisms of Cancer	5.06	N/A
Integrin Signalling	4.84	1.23
Hereditary Breast Cancer Signalling	4.80	N/A
Role of BRCA1 in DNA Damage Response	4.79	1.13
Huntington's Disease Signalling	4.44	0.00
ATM Signalling	4.29	0.00
HIPPO Signalling	4.29	-0.71
Remodelling of Epithelial Adherens Junctions	4.26	1.00
Sertoli Cell-Sertoli Cell Junction Signalling	4.11	N/A
Germ Cell-Sertoli Cell Junction Signalling	4.04	N/A
Death Receptor Signalling	4.00	-0.78
Axonal Guidance Signalling	3.92	N/A
mTOR Signalling	3.82	-0.54
Pancreatic Adenocarcinoma Signalling	3.65	1.29
GADD45 Signalling	3.50	N/A
Amyloid Processing	3.48	0.00
B Cell Receptor Signalling	3.46	0.85
Calcium Signalling	3.39	0.50
Telomerase Signalling	3.37	-0.91
Apoptosis Signalling	3.31	1.94
Breast Cancer Regulation by Stathmin1	3.30	N/A
Regulation of eIF4 and p70S6K Signalling	3.29	-0.71
FAK Signalling	3.27	N/A
NRF2-mediated Oxidative Stress Response	3.08	-0.58
Signalling by Rho Family GTPases	3.02	1.96
Cyclins and Cell Cycle Regulation	2.98	-1.00
Tight Junction Signalling	2.88	N/A
ERK/MAPK Signalling	2.82	0.00
Actin Cytoskeleton Signalling	2.77	0.63
Hypoxia Signalling in the Cardiovascular System	2.74	0.45
Phospholipase C Signalling	2.74	-1.04
IL-6 Signalling	2.73	0.50
HGF Signalling	2.72	2.32
ILK Signalling	2.71	0.22
Production of Nitric Oxide and Reactive Oxygen Species in Macrophages	2.68	-0.22
PI3K/AKT Signalling	2.67	-1.94
Protein Kinase A Signalling	2.66	0.56
Chronic Myeloid Leukemia Signalling	2.64	N/A

Table 2. Top 30 of 71 significant canonical pathways, as assessed by IPA using transcripts mapping only to the mouse genome, in Allo-aca-treated tumour xenografts (as compared to Veh), based on –log(*P*). *Immune/stress/inflammation; ^Metabolism/signalling themes

Ingenuity Canonical Pathways	**-log(*P*)**	**z-score**
IL-7 Signalling Pathway*	3.01	**2.24**
B Cell Receptor Signalling*	2.92	0.45
Role of Macrophages, Fibroblasts & Endothelial Cells- Rheumatoid Arthritis*	2.83	N/A
Cholecystokinin/Gastrin-mediated Signalling^	2.7	-0.45
Endocannabinoid Cancer Inhibition Pathway^	2.7	0.00
4-1BB Signalling in T Lymphocytes*	2.63	N/A
Remodelling of Epithelial Adherens Junctions	2.59	N/A
GNRH Signalling	2.51	0.45
BER Pathway*	2.37	N/A
Phospholipase C Signalling^	2.35	0.45
Phagosome Formation*	2.31	N/A
PI3K Signalling in B Lymphocytes*	2.25	0.45
ILK Signalling	2.21	-0.45
Haematopoiesis from Pluripotent Stem Cells	2.11	N/A
CCR5 Signalling in Macrophages*	2.09	N/A
Primary Immunodeficiency Signalling*	2.08	N/A
Glutamine Biosynthesis I^	2.08	N/A
Epithelial Adherens Junction Signalling	2.08	N/A
Communication between Innate and Adaptive Immune Cells*	2.08	N/A
Osteoarthritis Pathway*	2.06	-1.00
TR/RXR Activation	2.05	N/A
D-myo-inositol (1,4,5)-trisphosphate Degradation^	2.02	N/A
1D-myo-inositol Hexakisphosphate Biosynthesis II ^	1.97	N/A
D-myo-inositol (1,3,4)-trisphosphate Biosynthesis^	1.97	N/A
Gαq Signalling	1.95	-1.00
VEGF Signalling	1.89	0.00
SAPK/JNK Signalling*	1.88	**2.00**
Methionine Degradation I (to Homocysteine)^	1.81	N/A
Superpathway of D-myo-inositol (1,4,5)-trisphosphate Metabolism^	1.78	N/A
Cysteine Biosynthesis III^	1.74	N/A

Figures:

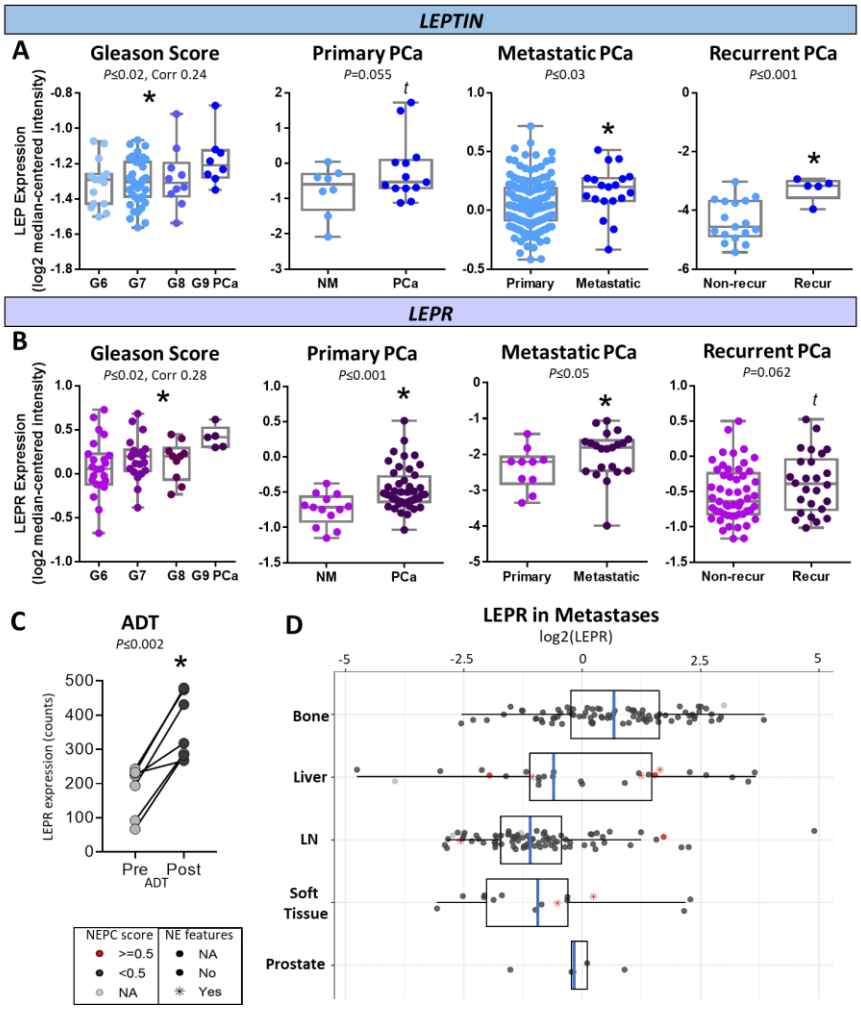

Figure 1 (A-D). Tumour leptin (*LEP*) and leptin receptor (*LEPR*) expression increases with PCa progression and in treatment resistant disease in patient samples. (A-B) *LEP* and *LEPR* expression evaluated in PCa patient samples using the Oncomine platform (transcriptomic and genomic datasets). ata represents **(A)** increased *LEP* expression in the Arredouani, Glinksy, Taylor 3 and Nanni patient datasets for primary vs non-malignant prostate, increasing Gleason score, metastatic vs localized PCa, recurrence vs non-recurrent at 1 yrs, respectively; and **(B)** increased *LEPR* expression in the Liu, La pointe, Chandran and Glinksy patient datasets for primary vs non-malignant prostate, increasing Gleason score, metastatic vs localized PCa, and recurrence vs non-recurrent at 1 yrs, respectively. Significant (**P*<0.05) and trending (^{t}*P*=0.055-0.07) *P*-values indicated. **(C)** *LEPR* expression evaluated

in the Rajan dataset in PCa biopsies profiled transcriptomically pre- and post-ADT (P<0.01). **(D)** *LEPR* expression evaluated in metastases in the Abida dataset, presented according to primary or metastatic tissue biopsy site and stratified according to NEPC score by color and neuroendocrine features by symbol, at localized or metastatic sites.

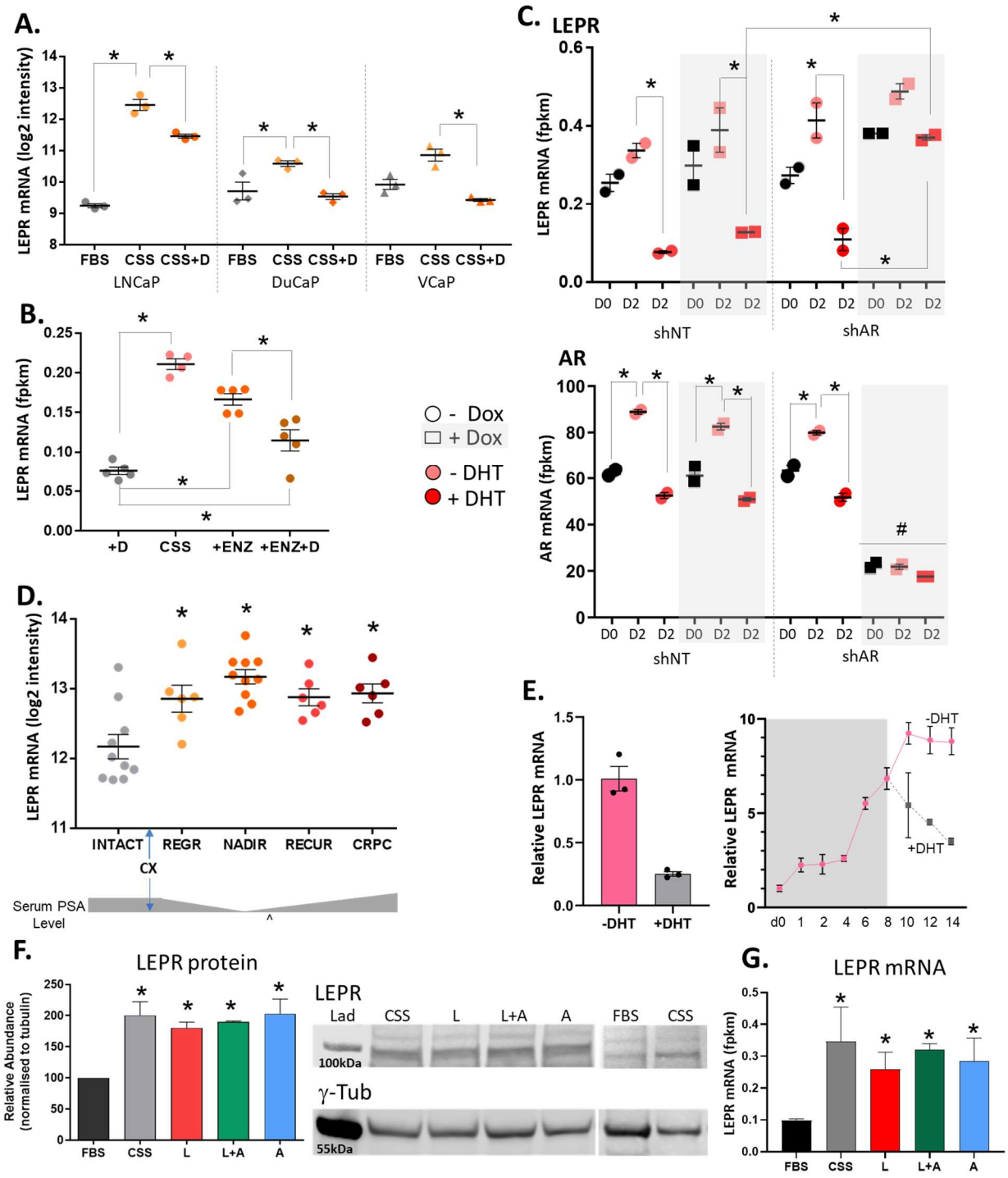

Figure 2 (A-G). Leptin receptor (*LEPR*) expression increases in cell lines subjected to androgen withdrawal *in vitro* and *in vivo*. (A) *LEPR* mRNA expression (by microarray) in LNCaP, DUCaP, VCaP PCa cell lines in normal growth media (FBS) or androgen deplete (Charcoal stripped serum, CSS) and replete (CSS + DHT) conditions. Significant: *$P \leq 0.05$. **(B)** *LEPR* mRNA expression (by RNAseq) in LNCaP cells in androgen deplete media (CSS) or androgen replete media (+D) ± androgen targeted (+ENZ) therapy. *$P \leq 0.05$. **(C)** *LEPR* mRNA expression (by RNAseq) in shAR LNCaP cells grown in androgen deplete media (CSS) ±treatment with doxycycline (Dox) for knockdown induction (shNT, shAR) and DHT for androgen replete conditions (upper panel). *AR* mRNA expression under Dox-induction demonstrates successful AR knockdown by inducible shAR

(lower panel, #$P \leq 0.05$ indicates validated knockdown in +Dox vs no Dox). Significant: *$P \leq 0.05$. **(D)** *LEPR* mRNA expression (by microarray) in an LNCaP prostate cancer progression xenograft model in mice. Xenografts were harvested from intact mice or mice that underwent castration with tumors collected at PSA progression points (Regression (REGR); Nadir, Recurrence (RECUR) orCastrate Resistance (CRPC)) . Significant: *$P \leq 0.05$, vs Intact; trend $^{T}P \leq 0.1$ vs CRPC. Progression of serum PSA across model time points indicated by schematic below. **(E)** Two independent experiments validating increased *LEPR* mRNA expression in androgen deplete conditions by qRT-PCR. Relative *LEPR* mRNA in LNCaP cells subjected to acute androgen deplete (CSS) or replete (CSS + DHT) conditions (n=1, mean ± SD) (left panel). Relative *LEPR* mRNA expression in LNCaP cells subjected to either normal growth media (FBS) (d0) or to chronic androgen deplete (CSS) conditions over up to 8 days. At day 8, cells were either maintained in androgen deplete (CSS) conditions or androgens were re-introduced (+DHT) for up to 6 days (n=1, mean ± SD) (right panel). **(F)** Human LEPR protein abundance measured in LNCaP PCa cell lysates relative to γ-tubulin loading control; densitometry was performed to quantify abundance from membrane total LEPR and background corrected. Cells were pretreated with ADT (CSS) for 48h and then subjected to 48h leptin (L, 10 nM) ± Allo-aca (A, 100 nM). Western blot, n=2; Lad = prestained protein ladder. Significant: *$P \leq 0.05$, vs FBS. (G) *LEPR* mRNA expression (by RNAseq) in LNCaP cells subjected to 2d androgen deplete media (CSS) or androgen rich media (FBS), followed by 48h (L, 10 nM) ± Allo-aca (A, 100 nM) treatment. Significant: *$P \leq 0.05$, vs FBS.

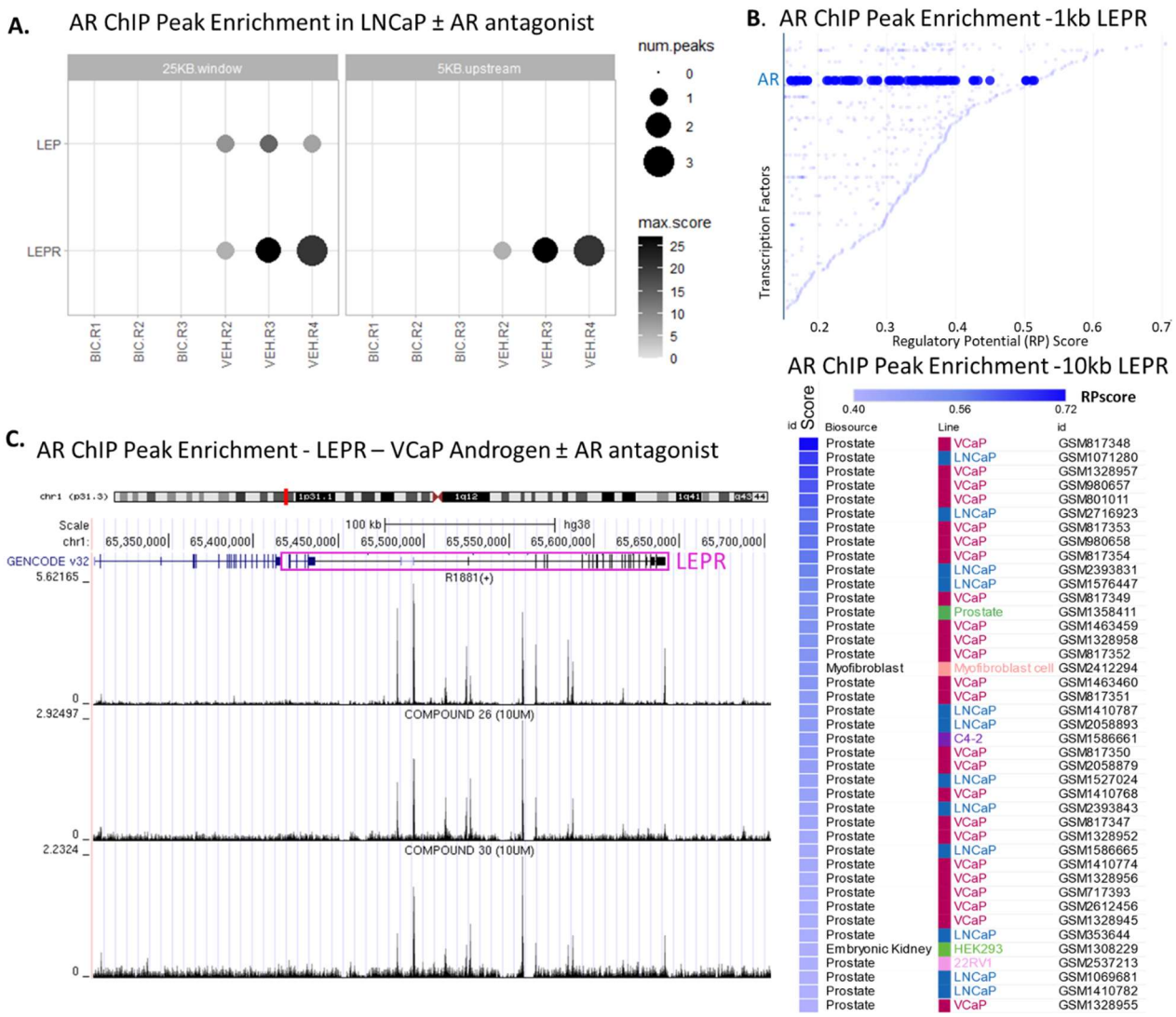

Figure 3 (A-C). Androgens regulate the expression of LEP and LEPR. (A) AR ChIPseq peak enrichment analysis of LEP and LEPR in the Ramos-Montoya data set of LNCaP cells treated with bicalutamide (BIC) compared with vehicle control. The number of peaks is highlighted by the bubble size and the enrichment score by the gray scale. **(B)** Regulatory potential (RP) score of AR analysed across datasets within the Cistrome database using AR ChIPseq peaks enriched within 1kb and 10kb of LEPR transcription start. Graph demonstrating AR RP score across samples compared to that of other transcription factors (y-axis) as a promoter-type transcription factor, within 1kb of LEPR transcription start. Heatmap detailing AR RP score across samples as an enhancer-type transcription factor, within 10kb of LEPR transcription start. **(C).** AR ChIPseq peaks displayed within and surrounding LEPR in the Zhu data set of VCaP cells and changes associated with small compound AR antagonist treatment (Compound 26, Compound 30) compared vehicle, androgen R1881 alone.

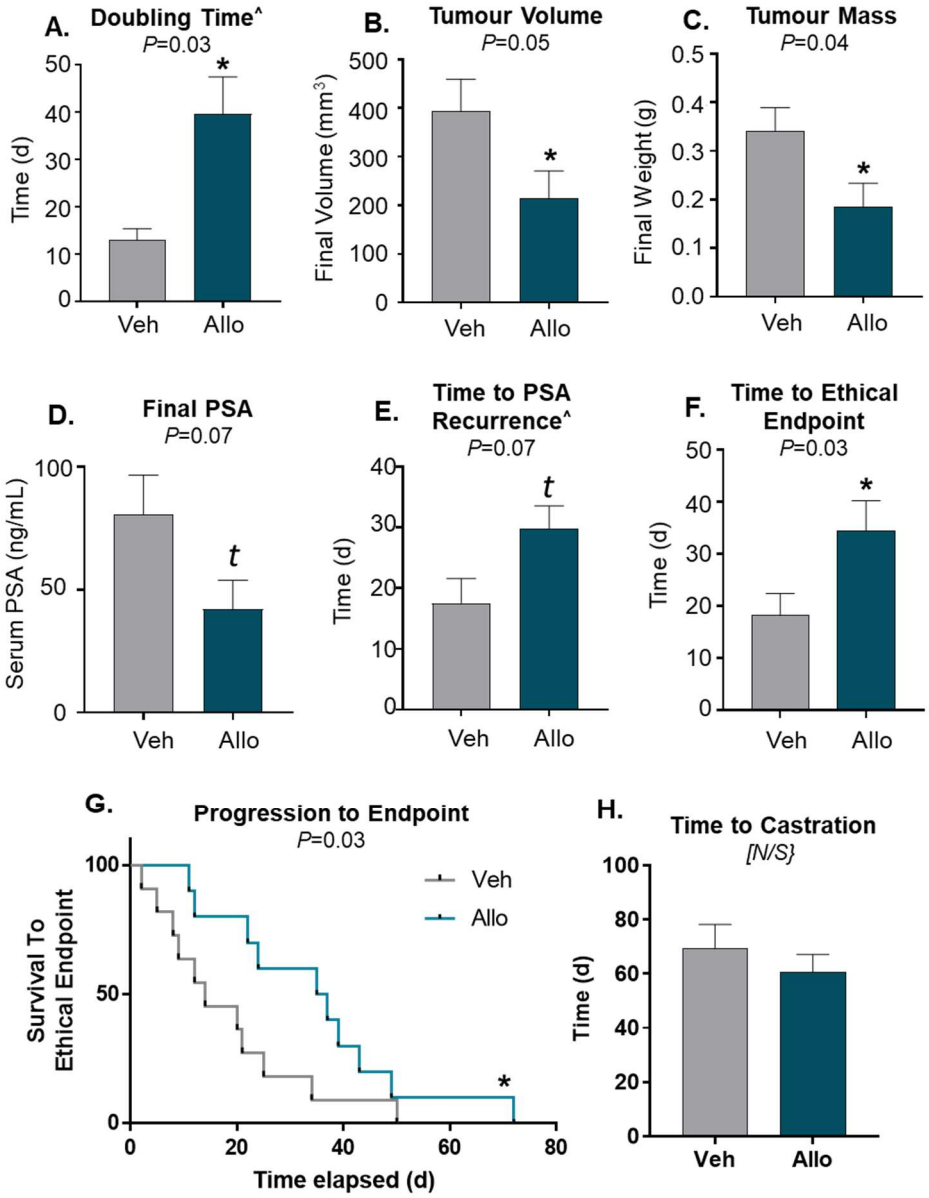

Figure 4 (A-H). Efficacious effects of Allo-aca in preventing tumour progression in LNCaP xenograft progression model in castrate Nude mice. Impact of Allo-aca on tumor xenograft **(A)** doubling time (^in cohort growth inhibition cohort n=5 Allo); **(B)** endpoint volume and **(C)** endpoint mass. **(D)** Serum PSA at endpoint and **(E)** time to PSA recurrence post-castration (^in cohort growth inhibition cohort n=5 Allo). **(F)** Time to ethical endpoint. **(G)** Progression to ethical endpoint by survival analysis. **(H)** Time to castration. Statistics: versus Veh, significant *$P \leq 0.05$ and trending ^{t} P=0.055-0.10; N/S, not significant; P-values indicated. n=11 vehicle (Veh), n=10 Allo-aca (Allo) unless indicated.

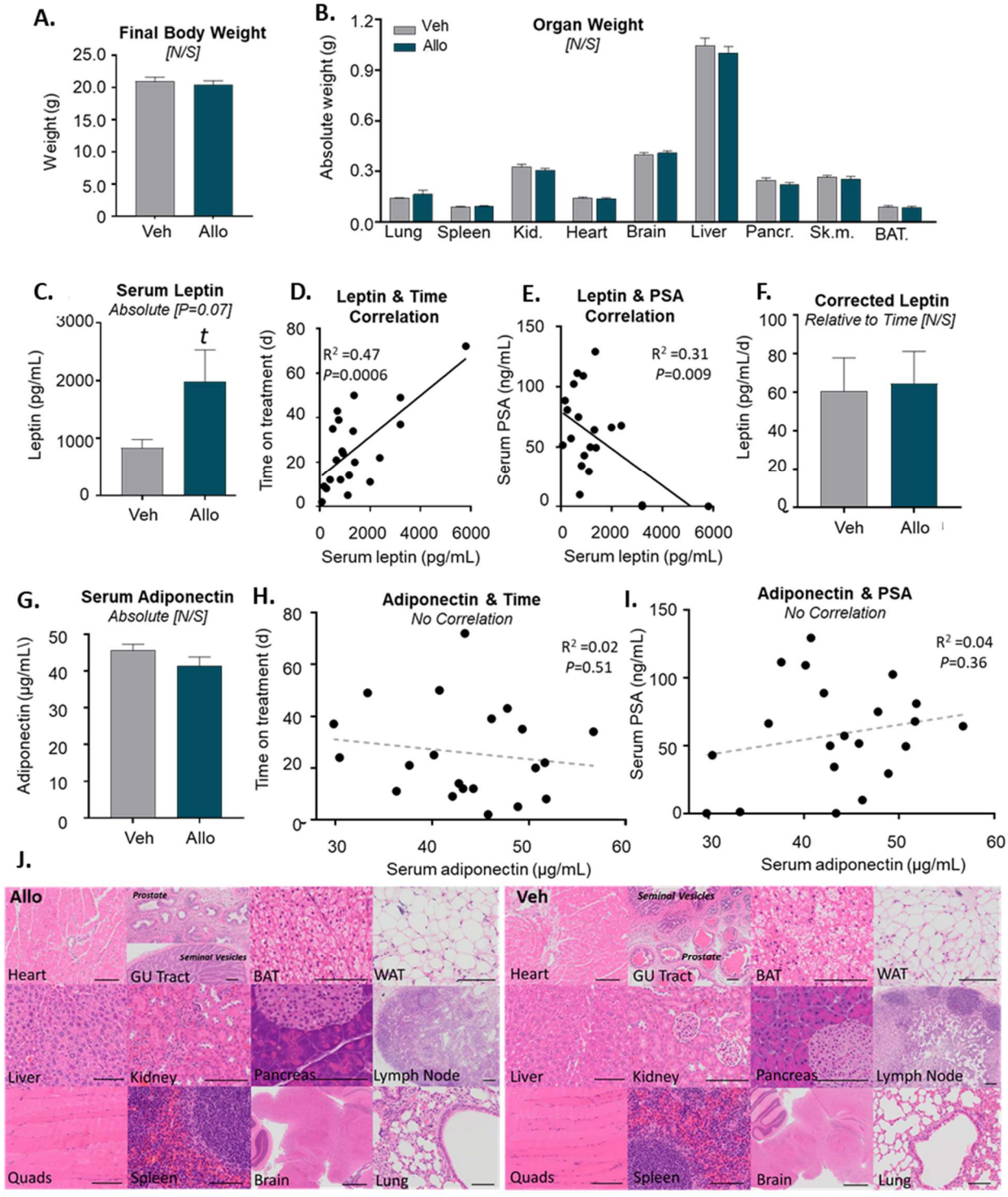

Figure 5 (A-J). Allo-aca had no impact on normal physiology and was well-tolerated in the LNCaP xenograft progression model in castrate Nude mice. Impact of Allo-aca (Allo) on mouse **(A)** body weight at endpoint; **(B)** absolute organ weight; **(C)** absolute serum leptin, compared to Vehicle (Veh). Assessment of correlation between serum leptin and **(D)** time on treatment, and **(E)** serum PSA in all mice. Impact of Allo on **(F)** serum leptin corrected for time on treatment, and **(G)** absolute serum adiponectin, compared to Veh. Assessment of correlation between serum adiponectin and **(H)** time on treatment, and **(I)** serum PSA in all mice. Statistics: versus Veh, significant **P*≤0.05 and trending ^{t}*P*=0.055-0.10; *P*-values indicated; N/S, not significant. n=11 vehicle (Veh), n=10 Allo-

aca (Allo) unless indicated. **(j)** Allo-aca has no effect on tissue pathology. Organ pathology by hematoxylin and eosin staining of heart, genitourinary (GU) tract (prostate and seminal vesicles indicated), brown (BAT) and white (WAT) adipose tissue, liver, kidney, pancreas, lymph node, muscle (quads, quadricep), spleen, brain and lung (scale bar = 100μm).

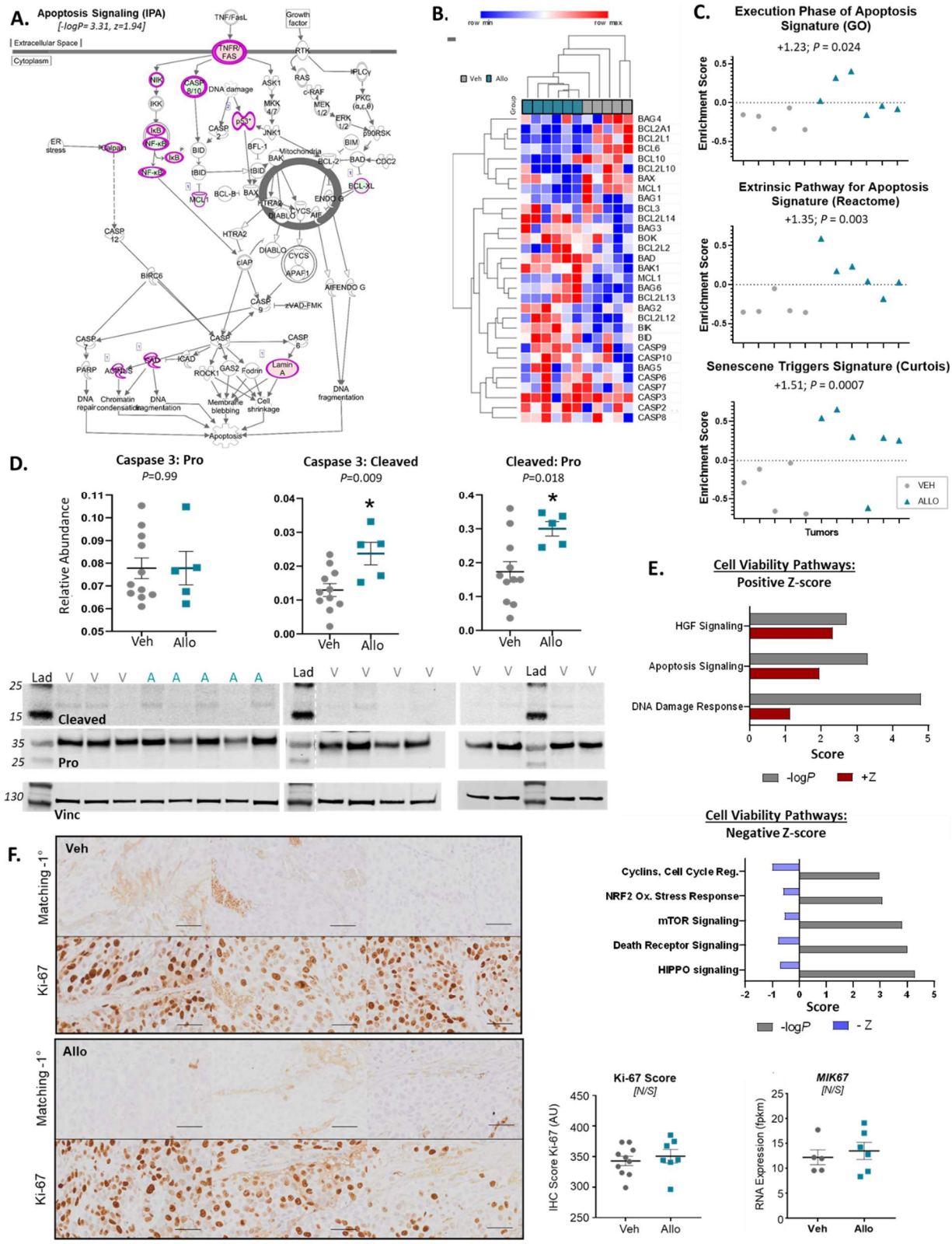

Figure 6 (A-F). Allo-aca impacts tumor xenograft apoptotic processes..) Pathway of apoptosis signalling, from IPA analysis of DE transcripts following tumor xenograft RNAseq. This map shows that apoptosis is a significantly affected canonical pathway induced by Allo-aca treatment. **(B)** Heatmap showing the expression of pro- and anti-apoptotic genes across tumor samples subjected to

RNAseq. **(C)** Significant enrichment of Curtois, 'GO' and Reactome molecular signatures within the Allo-aca transcriptomic dataset (mapped to human) related to apoptosis and cellular senescence. Enr = enrichment. Statistics: $^{*}P<0.05$, trend $^{T}P=0.055$-0.10, *P*-values indicated; n= 5 Veh, n=6 Allo. **(D)** Protein abundance of apoptotic marker, cleaved caspase 3 (active apoptosis) and pro-caspase 3, relative to vinculin loading control in tumour xenograft lysates. Densitometry was performed to quantify abundance from membrane; cleaved caspase detection of bands at ~17, 19 kDa and pro-caspase at ~35kDa was expressed relative to vinculin (~125kDa) and background corrected. Western blot, n=11 Veh, n=5 Allo; Lad = prestained protein ladder. Statistics: $^{*}P<0.05$, *P*-values indicated. **(E)** Cell viability-associated pathways detected as significantly altered by Z-score and -logP according to IPA analysis. **(F)** Representative images of 3 tumors probed for Ki-67 proliferative marker by immunohistochemistry. Ki-67 positive cells are stained brown (DAB), light counterstain with hematoxylin (scale bar =50μm). Minus primary antibody (-1°) matching area for Ki-67 staining provided above Ki-67 stained images to show specificity of Ki-67 staining. Ki-67 score, based on intensity and positivity, derived from tumor sections probed by immunohistochemistry with antibody raised against human Ki-67. Statistics, not significant (N/S); Veh (vehicle), n=10, Allo-aca (Allo) n=7**.** Expression of human Ki-67 gene, *MIK67*, in RNAseq from Allo-aca and Vehicle-treated tumors (fpkm); Statistics, not significant (N/S).

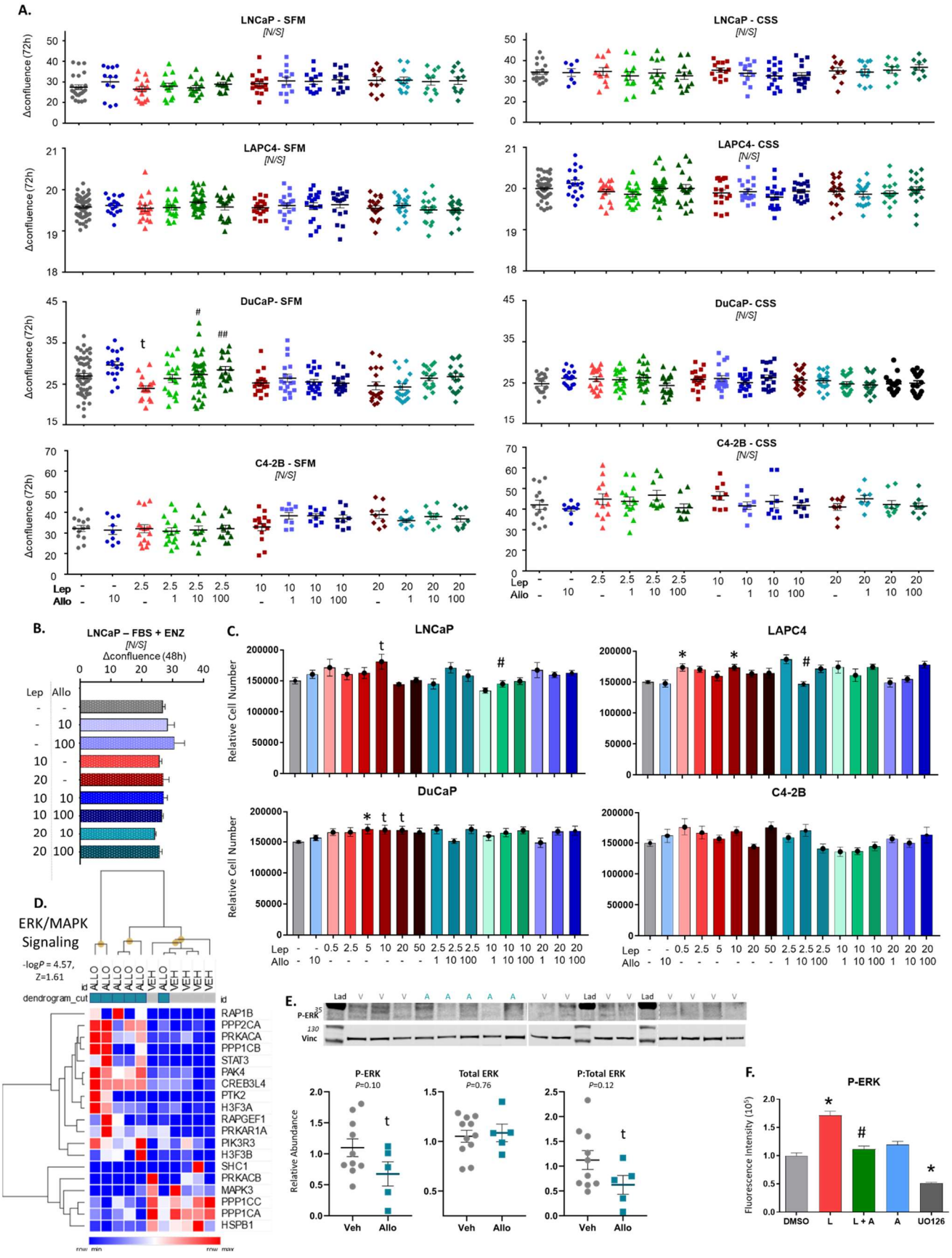
A.
LNCaP - SFM
[N/S]
LNCaP - CSS
[N/S]
LAPC4- SFM
[N/S]
LAPC4- CSS
[N/S]
DuCaP- SFM
DuCaP- CSS
[N/S]
C4-2B - SFM
[N/S]
C4-2B - CSS
[N/S]
Δconfluence (72h)
Lep
Allo
B.
LNCaP – FBS + ENZ
[N/S]
Δconfluence (48h)
C.
LNCaP
LAPC4
DuCaP
C4-2B
Relative Cell Number
D.
ERK/MAPK Signaling
-logP = 4.57,
Z=1.61
dendrogram_cut
RAP1B
PPP2CA
PRKACA
PPP1CB
STAT3
PAK4
CREB3L4
PTK2
H3F3A
RAPGEF1
PRKAR1A
PIK3R3
H3F3B
SHC1
PRKACB
MAPK3
PPP1CC
PPP1CA
HSPB1
E.
P-ERK
Vinc
P-ERK
P=0.10
Total ERK
P=0.76
P:Total ERK
P=0.12
Relative Abundance
Veh
Allo
F.
P-ERK
Fluorescence Intensity (10⁵)
DMSO
L
L + A
A
UO126

Figure 7 (A-F). Effect of leptin and Allo-aca on androgen-deprived PCa cell growth *in vitro*. (A) Change in confluence following 72h treatment with leptin (0, 2.5, 10, 20 nM) ± Allo-aca (0, 1, 10, 100nM) in androgen-deprived conditions in LNCaP, LAPC4, DuCaP, and C4-2B cells that had been pre-subjected to 48h androgen deprivation (media supplemented with charcoal stripped serum (CSS) or serum free media supplemented with BSA). Confluence 72h post-drug treatment, measured by IncuCyte, was represented relative to pretreatment confluence at time 0h. n=3; N/S, not significant. **(B)** Change in confluence following 48h treatment with leptin (0, 10, 20 nM) ± Allo-aca (0, 10, 100nM) in FBS ± Enzalutamide conditions in LNCaP cells that had been pre-subjected to 48h ATT (FBS media supplemented with Enzalutamide (10μM)). Confluence 48h post-drug treatment, measured by IncuCyte, was represented relative to pretreatment confluence at time 0h. n=1; N/S, not significant. **(C)** Cell number was assessed by DNA content using CyQuant (n=3) and expressed relative to pre-treatment values. Data represent LNCaP, DuCaP, LAPC4 and C4-2B cell lines exposed to 72h treatment with leptin (0, 0.5, 2.5, 5, 10, 20, 50 nM) ± Allo-aca (0, 1, 10, 100nM) in androgen-deprived conditions (CSS), with cells subjected to 48h androgen deprivation (media supplemented with charcoal stripped serum (CSS) prior to drug treatment. * $P<0.05$, vs CSS; # $P<0.05$, vs leptin dose alone; t trend, $P<0.1$. **(D)** Heatmap showing significant changes to ERK/MAPK signalling genes across tumor samples subjected to RNAseq. **(E)** Protein abundance of phospho (P-) ERK and total ERK, relative to vinculin loading control in tumor xenograft lysates. Densitometry was performed to quantify abundance from membrane; ERK detection of bands at 44/42 kDa (total, red channel; P-, green channel) was expressed relative to vinculin (~125kDa) and background corrected. Western blot, n=11 Veh, n=5 Allo; Lad = prestained protein ladder. Statistics: trend ^{t} $P=0.055$-0.10, P-values indicated; N/S, not significant. **(F)** Alpha-screen assessment of ERK signaling in LNCaP cells treated with leptin (20nM) ± Allo-aca (100nM) compared to controls (DMSO, U0126 (selective MEK1, 2 inhibitor, to inhibit the Ras/Raf/MEK/ERK signalling pathway)). Statistics: * $P<0.05$, vs DMSO; # $P<0.05$, vs leptin dose alone.

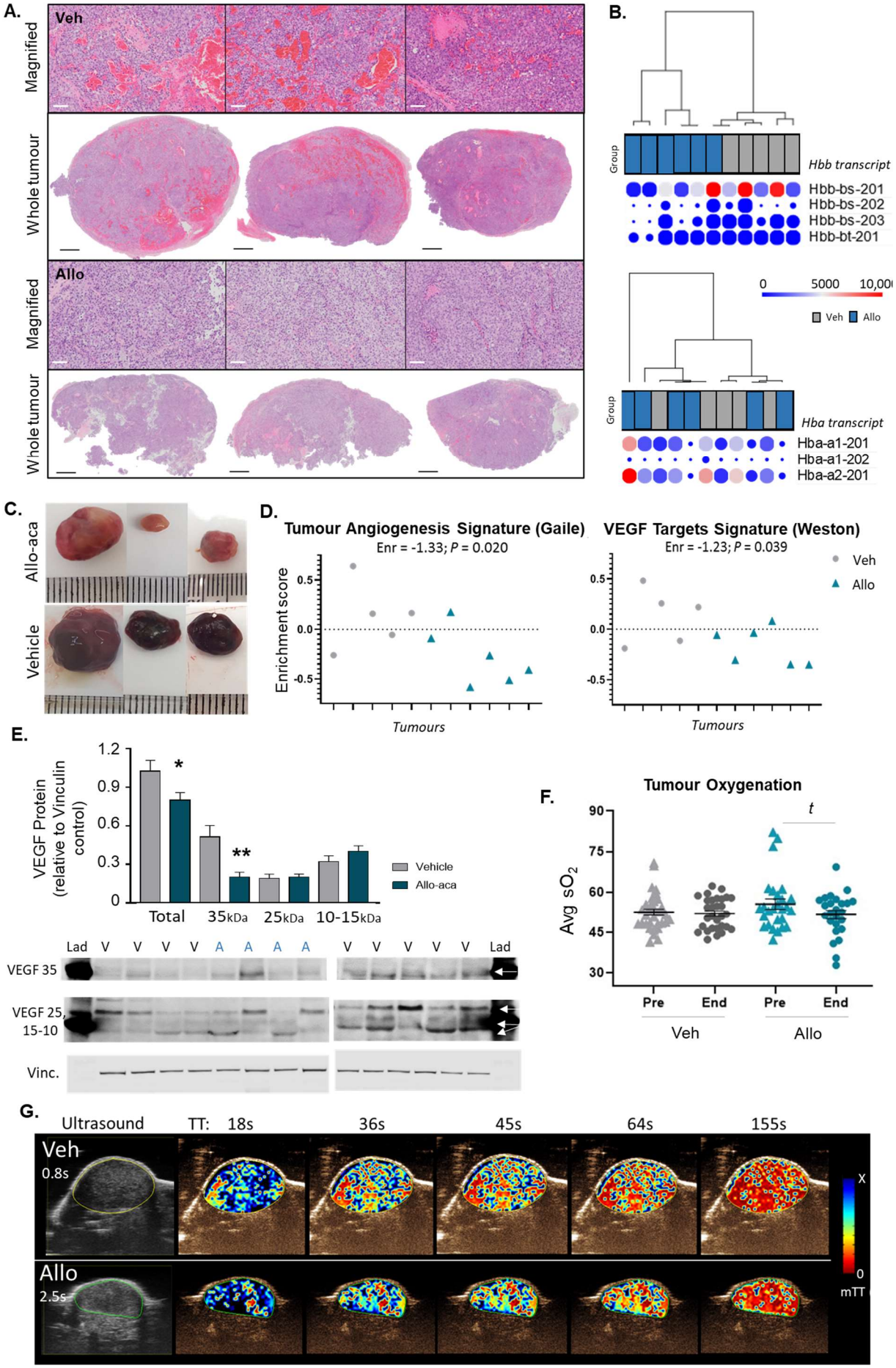
A.
Veh
Magnified
Whole tumour
Allo
Magnified
Whole tumour
B.
Group
Hbb transcript
Hbb-bs-201
Hbb-bs-202
Hbb-bs-203
Hbb-bt-201
0
5000
10,000
Veh
Allo
Group
Hba transcript
Hba-a1-201
Hba-a1-202
Hba-a2-201
C.
Allo-aca
Vehicle
D.
Tumour Angiogenesis Signature (Gaile)
Enr = -1.33; P = 0.020
Enrichment score
0.5
0.0
-0.5
Tumours
VEGF Targets Signature (Weston)
Enr = -1.23; P = 0.039
0.5
0.0
-0.5
Tumours
Veh
Allo
E.
VEGF Protein (relative to Vinculin control)
1.2
0.9
0.6
0.3
0
*
**
Total
35kDa
25kDa
10-15kDa
Vehicle
Allo-aca
Lad V V V V A A A A V V V V V Lad
VEGF 35
VEGF 25, 15-10
Vinc.
F.
Tumour Oxygenation
Avg sO2
90
75
60
45
30
t
Pre
End
Pre
End
Veh
Allo
G.
Ultrasound
TT:
18s
36s
45s
64s
155s
Veh
0.8s
Allo
2.5s
X
0
mTT

Figure 8 (A-G). Effect of Allo-aca on tumor xenograft phenotype and host microenvironment. **(A)** Tumor pathology by hematoxylin and eosin staining (scale bar: whole tumor = 1mm; magnified view =100μm); **(B)** Abundance of mouse transcripts for hemoglobin (beta (*Hbb*); alpha (*Hba*)) across tumor samples subjected to RNAseq; **(C)** Representative endpoint images showing Allo-aca altered tumor xenograft phenotype compared to Vehicle (ruler ticks at 1mm intervals); **(D)** Significant enrichment of molecular signatures within the Allo-aca transcriptomic dataset (mapped to human) related to angiogenesis. **(E)** Human VEGF protein abundance measured in tumor xenograft lysates relative to vinculin loading control; densitometry was performed to quantify abundance from membrane VEGF detection of bands at 35kDa, 25 kDa and at ~ 10,15 kDa and the sum of all protein (total). Vinculin (~125kDa) was used as a loading control. Lad = prestained protein ladder. Statistics: versus Veh, significant **P*≤0.05, ***P*<0.01. RNAseq, n=6 Allo-aca (Allo), n=5 Vehicle (Veh); Western blot, n=11 Veh, n=4 Allo. (F) Average sO_2 content at endpoint (compared to pretreatment) by live longitudinal PA spectral imaging of tumours, n=9 Allo, n=11 Veh; trend ^{t}P=0.12. (G) Perfusion in Veh and Allo-aca endpoint tumours (n=1) demonstrated using US contrast agent replenishment (transit time (TT) (s), colour scale X = maximum TT for that image).

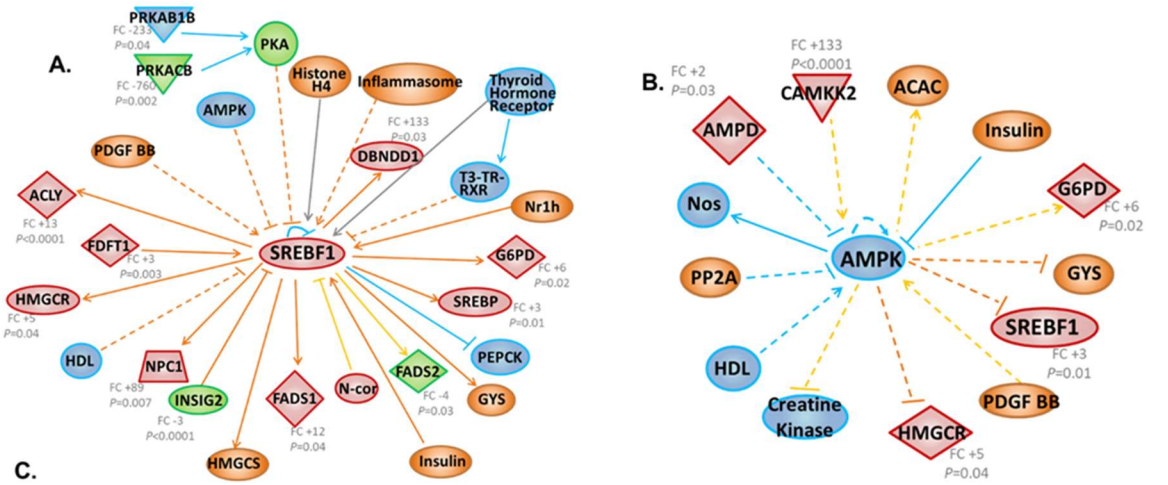

C.

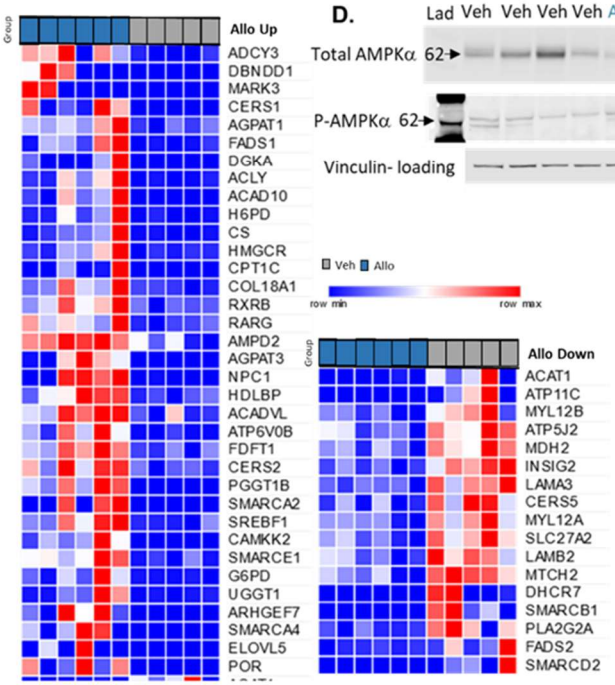

D.

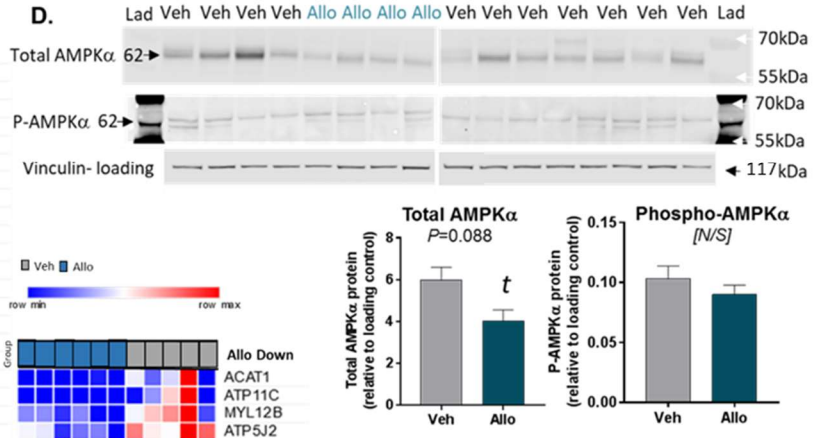

E.

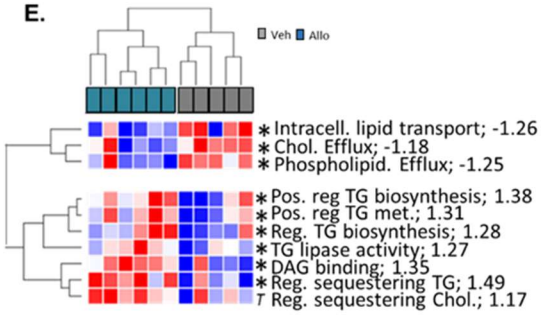

F.

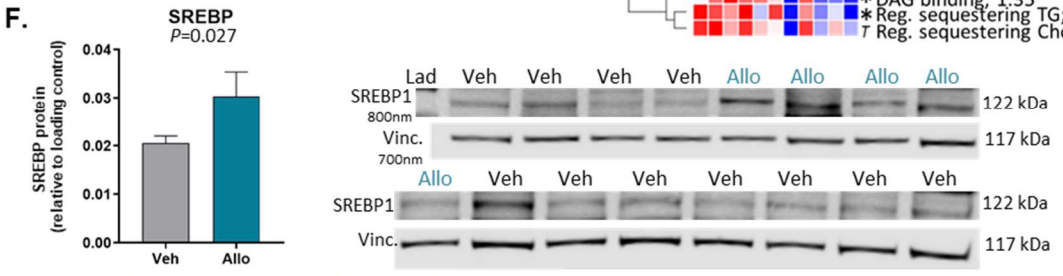

G.

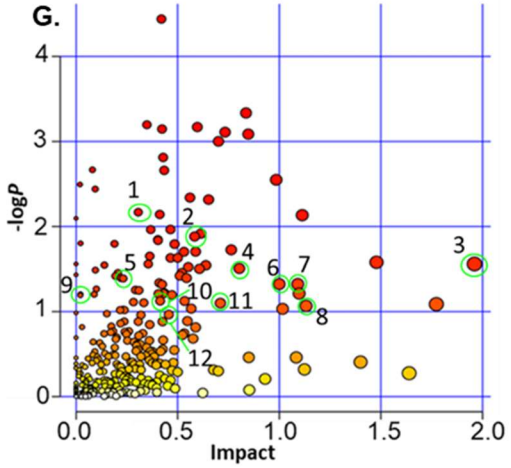

	Pathway	Rank	Hits	-log10*P*	Impact
1	Insulin signalling	15	18/137	2.34	0.560
2	Riboflavin met.	24	3/8	1.88	0.583
3	Purine met.	39	15/130	1.56	1.960
4	Alanine, aspartate, glutamate met.	43	6/36	1.51	0.803
5	Central carbon met.	51	9/69	1.39	0.221
6	Pentose phosphate	55	5/30	1.32	1.000
7	TCA cycle	56	5/30	1.32	1.091
8	Pyrimidine met.	75	7/57	1.07	1.132
9	Ox. phosphorylation	65	14/133	1.20	0.022
10	Glycosphingolip. met.	69	3/15	1.12	0.415
11	Glutathione metab.	73	7/56	1.10	0.710
12	Cysteine methionine	83	6/49	0.96	0.456

Figure 9(A-G). Effect of Allo-aca on cholesterol and lipid synthesis, and metabolic networks, in tumor xenografts derived from gene function analysis of RNAseq data using IPA and MetaboAnalyst. (A) "Lipid Metabolism, Small Molecule Biochemistry, Vitamin and Mineral Metabolism" identified as a key network significantly affected by Allo-aca (as compared to Vehicle); featuring upregulation of Master lipogenic regulator, SREBF1 and altered expression of several lipid and glucose metabolism enzymes. **(B)** Predicted AMPK suppression within the **"**Lipid Metabolism, Small Molecule Biochemistry, Vitamin and Mineral Metabolism" network; a potential mechanism for enhanced SREBF1 expression and predicted activity. **(C)** Heatmap representing altered expression of genes associated with lipid metabolism and AMPK signaling pathways from RNAseq analysis across Allo-aca-treated tumors, vs Vehicle (Veh) control; as identified in IPA analysis shown in (A) and (B). (A-C) Statistics: significant adjusted P-value $P \leq 0.05$, fold change (FC) cut off > +1.5, <-1.5. RNAseq, n=6 Allo-aca (Allo), n=5 Veh. Legend – red = upregulated, green = downregulated, orange = predicted upregulated based on pathway activation, blue = predicted downregulated based on pathway activation. **(D)** Protein abundance of total AMPKα and phospho (P-) AMPKα, relative to vinculin loading control in tumor xenograft lysates. Densitometry was performed to quantify abundance from membrane; AMPK detection of bands at 62kDa (total, red channel; P-, green channel) was expressed relative to vinculin (~117kDa) and background corrected. Western blot, n=11 Veh, n=4 Allo; Lad = prestained protein ladder. Statistics: trend ^{t} P=0.055-0.10, P-values indicated; N/S, not significant. **(E)** Significant enrichment of several 'GO' molecular signatures within the Allo-aca transcriptomic dataset (mapped to human) related to lipid metabolism and transport. Listed pathway; enrichment score. Statistics: *P<0.05, trend T P=0.055-0.10. **(F)** Protein abundance of SREBP1, relative to vinculin loading control in tumor xenograft lysates. Densitometry was performed as above 122kDa SREBP1 was expressed relative to vinculin (~117kDa) and background corrected. Western blot, n=11 Veh, n=5 Allo. Statistics: P-values indicated. **(G)** Other metabolic pathways (not lipid centric) that were also observed to be significantly enriched in MetaboAnalyst analyses of the Allo-aca-treated tumour transcriptome. Highlighted metabolism (met.) pathways are indicated by numbers alongside green circled nodes on the graph and details seen in the corresponding table. Node size corresponds to impact score while node colour corresponds to -log10P significance.

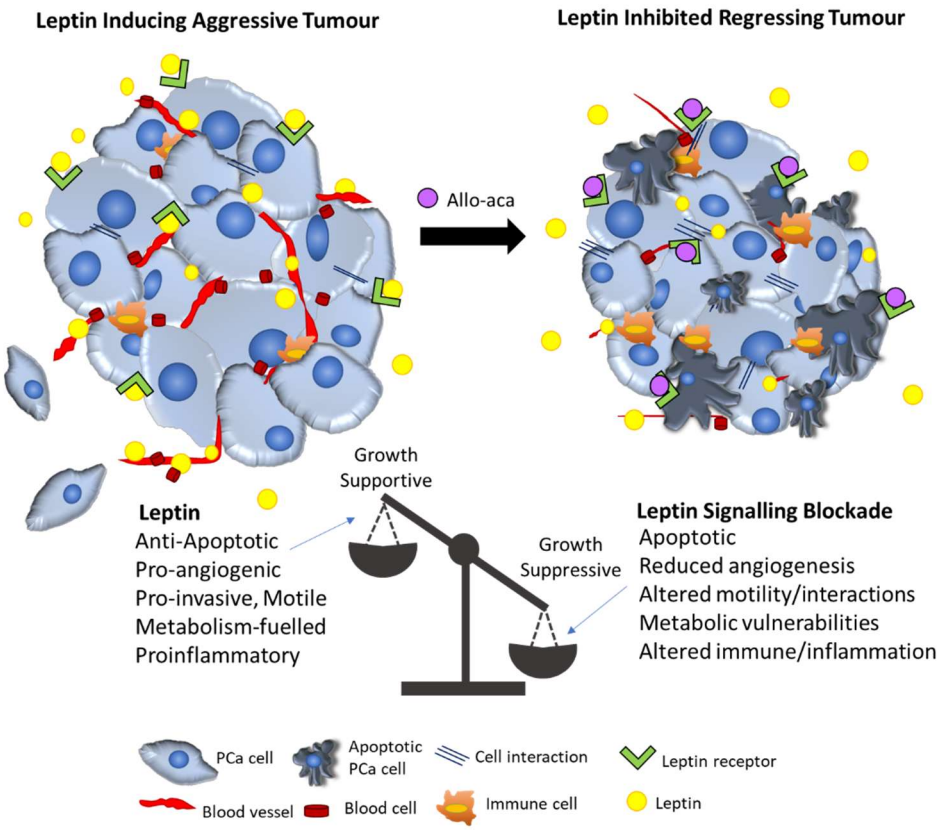

Figure 10. Schematic of leptin impacts on tumor xenograft phenotype and microenvironment and potential mechanisms highlighted to underlie anti-tumour efficacy of leptin signalling blockade by Allo-aca. Our and previous research supports leptin eliciting effects on the tumour and its microenvironment that are supportive of tumour growth and aggressiveness. This study has informed potential mechanisms of the growth limiting actions of Allo-aca on prostate tumours, which include induction of apoptosis, decreased tumour angiogenesis, altered tumour immune/inflammatory environment and rewired metabolism.

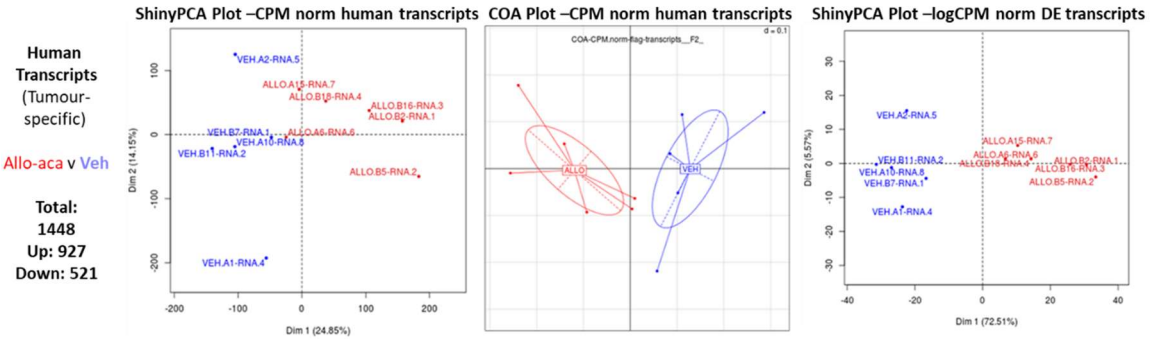

Suppl Fig1. Human transcripts (tumour-specific) from Allo-aca (Allo) and Vehicle (Veh) treated tumors cluster separately in PCA plots of normalized CPM of human transcripts, COA plots of normalized CPM of human transcripts and PCA plots of normalized logCPM of differentially expressed (DE) human transcripts. 1448 DE human transcripts were observed with Allo-aca treatment.

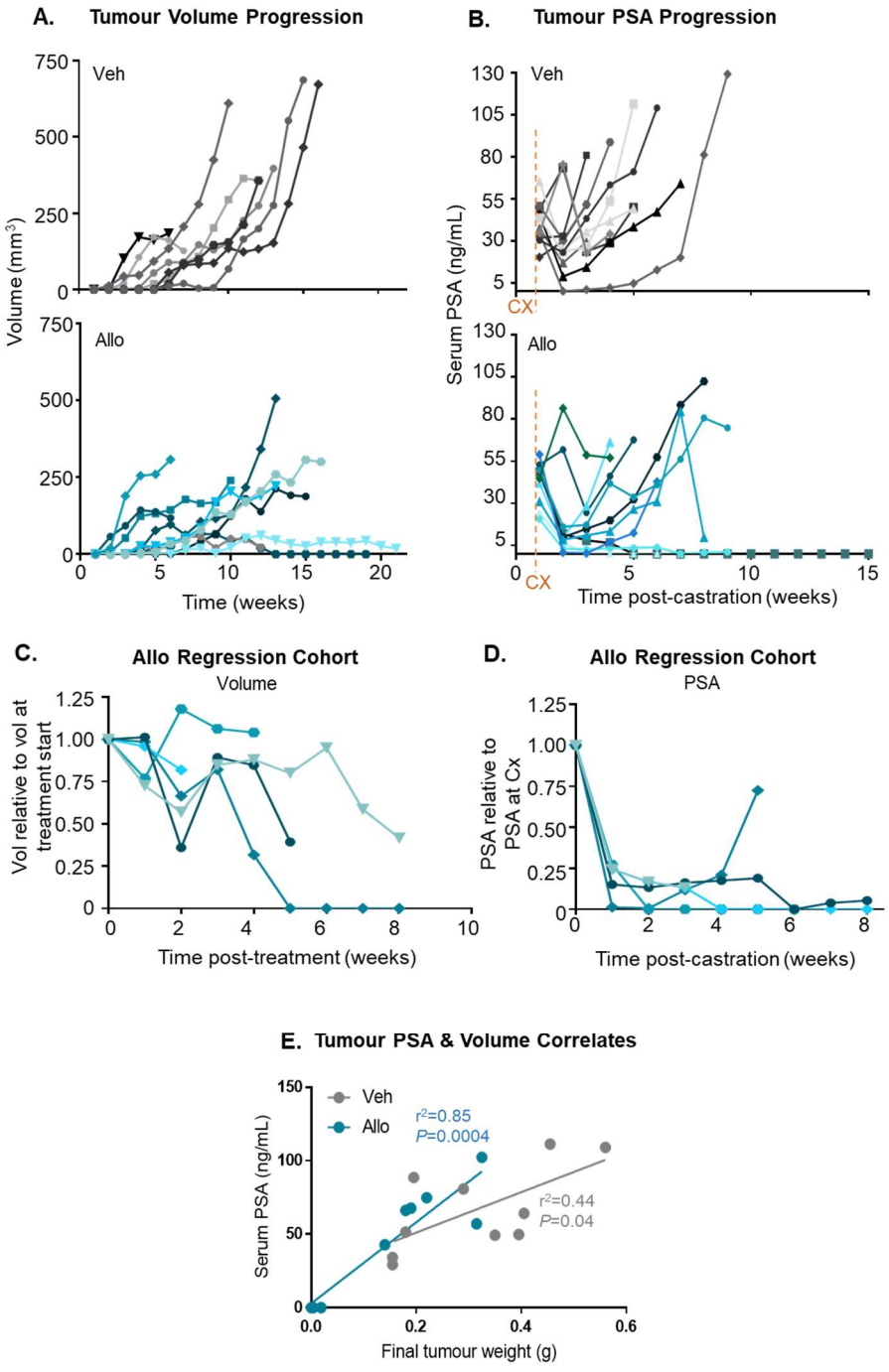

Suppl Fig2(A-E). Allo-aca efficacy in LNCaP xenograft progression model in castrate Nude mice. Progression over time of **(A)** tumor xenograft volume from day 0 and **(B)** serum PSA from castration. Regression over time of **(C)** tumor volume and **(D)** serum PSA in the Allo regression cohort n=5). **(E)** Correlation of endpoint tumor PSA and volume. Cx = castration.

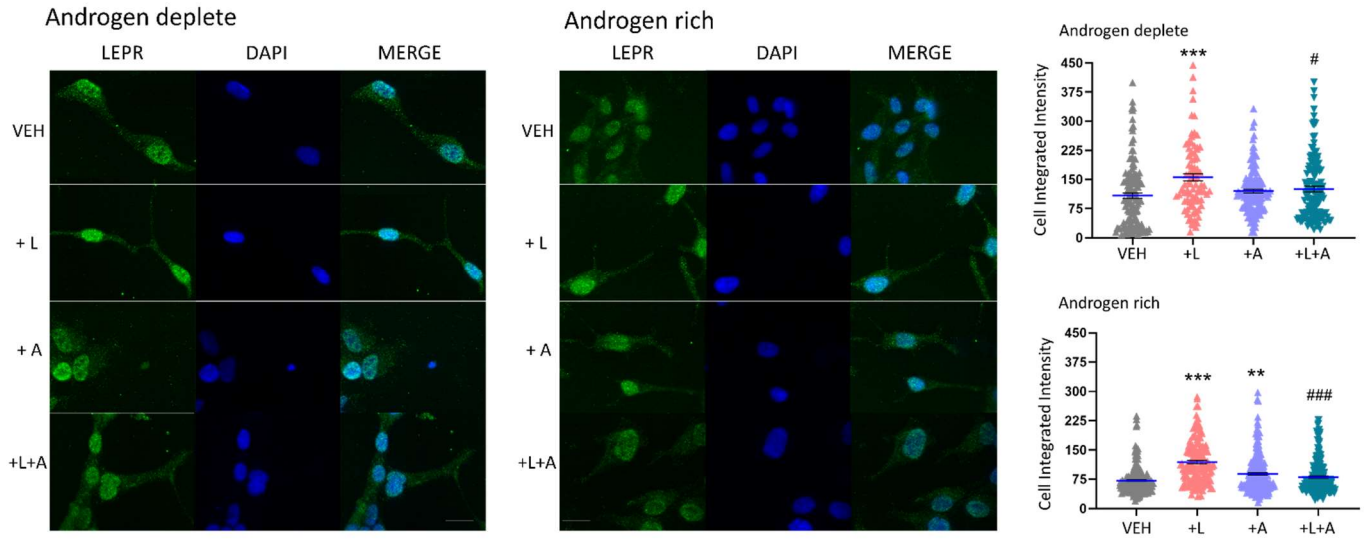

Suppl Fig3. Impact of leptin and Allo-aca on LNCaP cell LEPR protein. Representative images of LEPR (green) protein by immunofluorescence in LNCaP cells treated with acute leptin (10 nM) and Allo-aca (100 nM) *in vitro* under androgen deplete (CSS) or rich (FBS) conditions. Graphically represented as overall LEPR intensity of cells as calculated by Cell Profiler analysis. Statistics: $^{**}P \leq 0.01$, $^{***}P \leq 0.001$ vs vehicle; $^{\#}P \leq 0.05$, $^{\#\#\#}P \leq 0.001$ vs leptin alone in that condition.

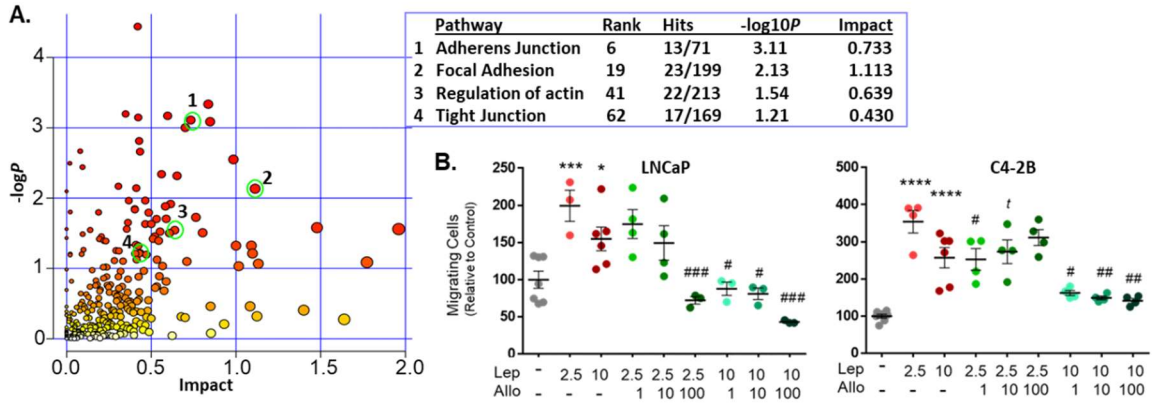

Suppl Figure 4 (A-B). Effect of Allo-aca on tumor xenograft phenotype and migration. (A) MetaboAnalyst gene-centric pathway analysis showing significant enrichment of pathways associated with cell adhesion/motility in Allo-aca treated tumours. Analysis was performed on differentially expressed transcripts mapping to the human genome. Pathways are indicated by numbers alongside green circled nodes on the graph and details seen in the corresponding table. Node size corresponds to impact score while node colour corresponds to -log10P significance. **(B)** Effect of leptin and Allo-aca on androgen-deprived PCa cell transwell migration in vitro. Relative number of migrating LNCaP and C4-2B cells following androgen-deprivation and treatment with leptin doses (0, 2.5, 10 nM), and leptin doses + Allo-aca (1, 10, 100nM); expressed relative to ADT vehicle control. n=3; Statistics: *P<0.05, ***P<0.001, ****P<0.0001, vs ADT vehicle; tP=0.055-0.10, #P<0.05, ##P<0.01, ###P<0.001, vs leptin dose alone.

SupplTable1. Top 25 expressed transcripts (based on fpkm value from RNAseq) mapping to the mouse genome expressed in tumour xenografts in Allo-aca (Allo) and Vehicle (Veh) treated mice. Mitochondrial transcripts – cell shaded grey. Transcript ID in superscript following gene symbol.

ALLO-ACA

	Allo1	Allo2	Allo3	Allo4	Allo5	Allo6
1	Co1^{-201}	Co1^{-201}	Co1^{-201}	Co1^{-201}	Hbb-bs^{-201}	Co1^{-201}
2	Atp8^{-201}	B2m^{-201}	Atp8^{-201}	B2m^{-201}	Hba-a2^{-201}	B2m^{-201}
3	Nd1^{-201}	Fth1^{-201}	Ftl1^{-201}	Atp8^{-201}	Co1^{-201}	Atp8^{-201}
4	Cytb^{-201}	Atp8^{-201}	Nd1^{-201}	Nd1^{-201}	Atp8^{-201}	Fth1^{-201}
5	B2m^{-201}	Lyz2^{-201}	Fth1^{-201}	Cytb^{-201}	Hba-a1^{-201}	Ftl1^{-201}
6	Nd4^{-201}	Cd74^{-201}	Cytb^{-201}	Cd74^{-201}	Ftl1^{-201}	Nd1^{-201}
7	Nd2^{-201}	Nd1^{-201}	Apoe^{-202}	Fth1^{-201}	Nd1^{-201}	Cd74^{-201}
8	Cd74^{-201}	Cytb^{-201}	Hbb-bs^{-201}	Nd4^{-201}	Cytb^{-201}	Cytb^{-201}
9	Apoe^{-209}	Apoe^{-209}	Apoe^{-209}	Eef1a1^{-201}	Fth1^{-201}	Apoe^{-202}
10	Fth1^{-201}	Ftl1^{-201}	Nd4^{-201}	Ftl1^{-201}	Apoe^{-202}	Hbb-bs^{-201}
11	Nd5^{-201}	Nd4^{-201}	Selenop^{-201}	Lyz2^{-201}	Apoe^{-209}	Nd4^{-201}
12	Ftl1^{-201}	Eef1a1^{-201}	Lyz2^{-201}	Nd2^{-201}	Nd4^{-201}	Eef1a1^{-201}
13	Eef1a1^{-201}	Nd5^{-201}	Nd2^{-201}	Apoe^{-209}	Eef1a1^{-201}	Apoe^{-209}
14	Atp6^{-201}	Ctss^{-202}	Eef1a1^{-201}	Nd5^{-201}	Nd2^{-201}	Lyz2^{-201}
15	Lyz2^{-201}	Nd2^{-201}	B2m^{-201}	Apoe^{-202}	B2m^{-201}	Nd2^{-201}
16	Co3^{-201}	Apoe^{-202}	Hba-a2^{-201}	Atp6^{-201}	Lyz2^{-201}	Hba-a2^{-201}
17	Fabp4^{-201}	Psap^{-203}	Sparc^{-202}	Bgn^{-201}	Sparc^{-202}	Nd5^{-201}
18	Col1a1^{-201}	Ctsd^{-202}	Nd5^{-201}	Eef1a1^{-204}	Ctsd^{-202}	Psap^{-202}
19	Actb^{-209}	H2-Ab1^{-201}	Col3a1^{-201}	Sparc^{-202}	Nd5^{-201}	Ctss^{-202}
20	Sparc^{-202}	Jchain^{-201}	Ctsd^{-202}	Tmsb4x^{-201}	Bgn^{-201}	Ctsd^{-202}
21	Co2^{-201}	Atp6^{-201}	Bgn^{-201}	Actb^{-201}	Col1a1^{-201}	Jchain^{-201}
22	H2-Ab1^{-201}	Psap^{-202}	Col1a1^{-201}	Co3^{-201}	Col3a1^{-201}	H2-Ab1^{-201}
23	Eef1a1^{-204}	Actb^{-209}	Col1a2^{-201}	Col1a1^{-201}	Selenop^{-201}	C1qb^{-201}
24	Tmsb4x^{-201}	Eef1a1^{-204}	Hba-a1^{-201}	Rps24^{-201}	Col1a2^{-201}	Hba-a1^{-201}
25	Ctss^{-202}	H2-Aa^{-201}	Gpx3^{-201}	Actb^{-209}	Co3^{-201}	Ly6e^{-215}

VEHICLE

	Veh1	Veh2	Veh3	Veh4	Veh5
1	Co1^{-201}	Co1^{-201}	Hbb-bs^{-201}	Co1^{-201}	Co1^{-201}
2	Fth1^{-201}	Hbb-bs^{-201}	Fth1^{-201}	Atp8^{-201}	Atp8^{-201}
3	Nd1^{-201}	Atp8^{-201}	Co1^{-201}	Nd1^{-201}	Nd1^{-201}
4	Atp8^{-201}	B2m^{-201}	Apoe^{-209}	Cytb^{-201}	B2m^{-201}
5	Cytb^{-201}	Nd1^{-201}	Ftl1^{-201}	Nd4^{-201}	Cytb^{-201}
6	Ftl1^{-201}	Cytb^{-201}	Hba-a2^{-201}	Fth1^{-201}	Nd4^{-201}
7	Apoe^{-209}	Hba-a2^{-201}	Atp8^{-201}	Nd2^{-201}	Apoe^{-209}
8	Nd4^{-201}	Nd4^{-201}	Nd1^{-201}	B2m^{-201}	Fth1^{-201}
9	B2m^{-201}	Hba-a1^{-201}	Cytb^{-201}	Ftl1^{-201}	Ftl1^{-201}
10	Nd2^{-201}	Fth1^{-201}	Hba-a1^{-201}	Nd5^{-201}	Nd2^{-201}
11	Lyz2^{-201}	Nd5^{-201}	Nd4^{-201}	Atp6^{-201}	Sparc^{-202}
12	Hbb-bs^{-201}	Nd2^{-201}	Lyz2^{-201}	Apoe^{-209}	Col1a1^{-201}
13	Eef1a1^{-201}	Eef1a1^{-201}	B2m^{-201}	Lyz2^{-201}	Col3a1^{-201}
14	Col3a1^{-201}	Atp6^{-201}	Apoe^{-202}	Eef1a1^{-201}	Bgn^{-201}
15	Sparc^{-202}	Apoe^{-209}	Eef1a1^{-201}	Bgn^{-201}	Eef1a1^{-201}
16	Ctsd^{-202}	Igfbp7^{-201}	Nd2^{-201}	Sparc^{-202}	Apoe^{-202}
17	Bgn^{-201}	Ftl1^{-201}	Ctsd^{-202}	Col1a1^{-201}	Nd5^{-201}
18	Col1a1^{-201}	Actb^{-209}	Bgn^{-201}	Co2^{-201}	Hbb-bs^{-201}
19	Hba-a2^{-201}	Cd74^{-201}	Sparc^{-202}	Selenop^{-201}	Col1a2^{-201}

20	Apoe-203	Sparc-202	Igfbp7-201	Actb-209	Actb-209
21	Apoe-202	Igfbp3-201	Apoe-203	Col3a1-201	Gpx3-201
22	Nd5-201	Eef1a1-204	Eef1a1-204	Co3-201	Igfbp3-201
23	Actb-209	Co2-201	Hmox1-201	Hmox1-201	Selenop-201
24	Col1a2-201	Lyz2-201	Actb-209	Ctsd-202	Lyz2-201
25	Selenop-201	Ctsd-202	Col1a1-201	Eef1a1-204	Cd74-201